



المملكة العربية السعودية
وزارة التعليم العالي
جامعة أم القرى
كلية العلوم التطبيقية
قسم الفيزياء

دراسة الخواص الضوئية
لأغشية رقيقة مختلفة التكوين
من الجرمانيوم-التيليريوم-النحاس

إعداد

غادة عبدالرحمن الزايد

إشراف

د. ناهد أبو الحسن القباني

أ.د. أحمد حمزة عرابي

رسالة مقدمة إلى قسم الفيزياء بكلية العلوم التطبيقية بجامعة أم القرى
كمطلب تكميلي لبرنامج درجة الماجستير في الفيزياء

1430 هـ - 2009 م

Kingdom of Saudi Arabia
Ministry of Higher Education
Umm Al-Qura University
Faculty of Applied Science
Department of Physics



**Study of Optical Properties of Ge-Te-Cu
Thin Films of
Different Compositions**

by

Ghada Abdulrahman Al-Zaidy

Supervised by

Prof. Dr. Ahmad H. Oraby

Dr. Nahed A. El-Kabany

A thesis submitted in partial fulfillment of the requirement for
the degree of Master of Science
(Physics)

1430H-2009G

ملخص الرسالة

تهدف هذه الدراسة إلى الحصول على نتائج حول تأثير تغيير التركيب لأغشية رقيقة مختلفة التكوين من الجيرمانيوم-تيلوريوم-نحاس $Ge_{15}Te_{85-x}Cu_x$ على الخواص الضوئية والالكترونية لها ولعل الهدف الأساسي من هذه الدراسة هو تطوير فهم طبيعة أشباه الموصلات الأمورفية وأيضا للحصول على أكبر قدر من الثوابت الضوئية والالكترونية عن طريق الدراسة العملية والنظرية من طيف الامتصاص والنفاذية لهذه العينات، ومن ثم تعيين العينة الأكثر كفاءة لاستخدامها في الدوائر الالكترونية .

وقد تم تحضير خمس عينات من $Ge_{15}Te_{85-x}Cu_x$ (بتركيزات مختلفة للنحاس والتيلوريوم) بطريقة التبخير الحراري. وللتحقق من الطبيعة الأمورفية للعينات تم اجراء قياسات حيود الأشعة السينية X-ray diffraction التي اكدت أن العينات جميعا كانت في الحالة الأمورفية.

ولدراسة خواص العينات الضوئية تم قياس طيف الامتصاص والنفاذية لهذه العينات في المدى 280-1000 nm ، ومنه حسبت بعض الثوابت الضوئية كقيمة فجوة الطاقة الضوئية ، عرض الحالات المحلية ، معامل الانكسار ، معامل التخميد، والجزء التخيلي والحقيقي لثابت العزل. ولقد وجدنا في الدراسات الطيفية ان الانتقال الالكتروني المباشر المسموح هو الانتقال ال مسؤول عن الامتصاص الضوئي وفسر هذا باستخدام علاقة توك Tauc's relation . ولقد وجد ان فجوة الطاقة الضوئية تصل إلى قيمة دنيا عند تركيز عنصر النحاس $x=5$ ، وسمي هذا التركيز بالتركيز الحرج critical composition.

تم دراسة تشتت معامل الانكسار في ضوء نموذج ويمبل دي دومينيك Single-Oscillator Wemple and DiDomenico Model حيث تم حساب قيمة كل من طاقة التشتت وطاقة المتذبذب وعلاقتهم بفجوة الطاقة الضوئية.

ولدراسة علاقة طاقة الفجوة الضوئية بالتركيب الكيميائي للعينات المحضرة تم حساب متوسط الطاقة الذرية ومتوسط رقم الاحداثي وربط هذه القيم بقيم طاقة الفجوة الضوئية.

وقد أظهرت النتائج أن متوسط الطاقة الذرية يزيد يقل بزيادة عنصر النحاس، وانه عند تركيز نحاس $x=5$ متوسط رقم احداثي يساوي 2.40 . هذا التركيز يعتبر التركيز الحرج الذي نجد تغيرات في جميع الثوابت الضوئية.

تم تفسير تغير طاقة الفجوة الضوئية بتغير التركيز باستخدام نظرية قيود الربط Bond Constraint Theory ونظرية الصلابة Rigidity Theory .

Abstract

A systematic investigation of the optical and structural properties of $\text{Ge}_{15}\text{Te}_{85-x}\text{Cu}_x$ ($2 \leq x \leq 6 \text{ at. \%}$) thin films was carried out. The aim of this work is to report information concerning the effect of composition on the optical properties of $\text{Ge}_{15}\text{Te}_{85-x}\text{Cu}_x$ ($2 \leq x \leq 6 \text{ at. \%}$) amorphous thin films. The films of $\text{Ge}_{15}\text{Te}_{85-x}\text{Cu}_x$ system ($2 \leq x \leq 6 \text{ at. \%}$) were prepared by thermal evaporation having the same thickness of 200 nm.

X-ray diffraction (XRD) measurements showed that the as-prepared $\text{Ge}_{15}\text{Te}_{85-x}\text{Cu}_x$ thin films were amorphous.

Transmittance and absorption measurements in the range of 280-1000 nm were used to determine the optical band gap E_g^{opt} , the width of localized states and more other optical constants like, refractive index (n), extinction coefficient (k) and the real and imaginary parts of the dielectric constant (ϵ_∞).

Changes in absorption spectra are directly correlated with variation in relative concentrations of the structure of the thin films. Analyzing the absorption spectra shows that optical absorption is due to indirect transitions, Tauc's relation for the allowed direct transition have been used to describe the optical transition in the studied films. The influence of composition on the optical band gap and the width of the band tail of thin films of chalcogenide glass system germanium-tellurium-copper (Ge-Te-Cu), was investigated.

It was shown that the optical gap decreases with the addition of copper in the binary Ge-Te-Cu system and reaches a minimum values $E_g^{opt} = 1.48 eV$ for $x = 5$ and this composition can be considered as a critical composition (threshold composition), of which the system becomes a chemically ordered alloy.

The dispersion of the refractive index was discussed in terms of the single-oscillator Wemple and DiDomenico model.

The relationship between E_g^{opt} and chemical composition in the $Ge_{15}Te_{85-x}Cu_x$ thin films was discussed in terms of the average heat of atomization (H_s) and related parameters such as the average coordination number ($\langle r \rangle$). An attempt has been made to evaluate this correlation according to simple criterion for computing the ability of a chalcogenide system to retain its vitreous states.

The results indicated that there was a correlation between the optical band gap, the average heat of atomization H_s and the average coordination number. It was clear that H_s decreases with Cu content increases. One observes that $\langle r \rangle$ reaches the value 2.40 at the copper content $x = 5$ indicated that this composition is a critical composition. The observed behavior of the optical properties in the range of compositions studied was explained on the basis of the Bond Constraint Theory (BCT) and Rigidity Theory.

Acknowledgments

First and foremost I owe my thanks to Allah for enabling me to undertake this dissertation that was undertaken at the Physics department, Faculty of Applied Science, Umm Al-Qura University, under the supervision of Prof. Dr. Ahmed Hamza Oraby and Dr. Nahed A. El-Kabany.

I would like to thank Prof. Dr. Ahmad Hamza Oraby and Dr. Nahed A. El-Kabany, for suggesting the subject, and providing me with all I needed for this study. I also offer my thanks to Prof. Dr. Ahmad Hamza Oraby for providing the technical support and experimental facilities from Faculty of Science, Mansoura University, Egypt.

I would like to express my thanks the Physics Department, Faculty of Applied Science, Umm Al-Qura University, for providing facilities required to complete this work.

I would like to thank King Abdul-Aziz City of Science and Technology (KACST), General Directorate of Research Grants Program for their encouragement and financial support. It gives me great pride to have this research (reference number GSP-17-174) among the fortunate researches that have been accepted by this special grant through its 17th Grants Program offered for graduate students in year 2009.

Last but not least this work would not have been possible without the love, encouragement, patience and support from my parents, my sisters and my dear brother.

Contents

Abstract	1
Acknowledgments	
Chapter 1. Introduction	3
Chapter2. Theoretical Considerations and Literature Survey	8
2.1. Introduction	9
2.2. Classification of optical processes	9
2.3. Amorphous chalcogenide glasses	13
2.3.1. Specifications of amorphous chalcogenide glasses	13
2.3.2. Structure study of amorphous chalcogenide semiconductors (Ge-Te-Cu alloy)	16
2.4. Optical Properties	17
2.4.1. Specifications of energy gap in amorphous semiconductors	17
2.4.2. Optical absorption edge	20
2.4.2.1. High Absorption region	22
2.4.2.2. The exponential region of the absorption edge	24

2.4.2.3. Weak Absorption Tail region (WAT)	25
2.4.3. Absorption Process (direct and indirect transitions)	25
2.4.3.1. Direct transition	27
2.4.3.2. Indirect transition	29
2.5. Optical constants	32
2.5.1. Refractive index (n) and extinction coefficient (k) and real and imaginary parts of high frequency dielectric constant	33
2.6. Dispersion of the refractive index within the Wemple-DiDomenico (WDD) single-oscillator dispersion model	38
2.7. Relation between optical energy gap and chemical composition	39
2.7.1. The average heat of atomization	40
2.7.2. The average coordination number	41
2.8. Literature Survey	43
2.8.1. Structure Study	43
2.8.2. Optical and physical properties of amorphous thin films	44
2.8.3. Composition dependence of the optical properties of amorphous thin films	47
2.8.4. Effect of addition of metals on optical properties of amorphous thin films	50
2.8.5. Effect of composition on the heat of atomization	51

Chapter 3. Experimental Techniques	53
3.1. Introduction	54
3.2. Material preparation	54
3.2.1. Preparation of bulk material $\text{Ge}_{15}\text{Te}_{85-x}\text{Cu}_x$	54
3.2.2 : Preparation of $\text{Ge}_{15}\text{Te}_{85-x}\text{Cu}_x$ thin films	56
3.3. Structure examination	57
3.3.1. X-Ray diffraction	57
3.4. Optical absorption measurements	58
Chapter 4. Results and Discussions	59
4.1. Introduction	60
4.2. Structure information	60
4.2.1. XRD (X-ray Diffraction)	60
4.3. Determination of optical constants of $\text{Ge}_{15}\text{Te}_{85-x}\text{Cu}_x$ thin films	61
4.3.1. Analysis of absorption coefficient	62
4.3.1.1. Determination of extinction coefficient	64
4.3.1.2. Lower values of absorption coefficient (determination of Urbach energy)	65
4.3.1.3. Higher values of absorption coefficient (determination of optical energy gap)	67

4.3.2. Determination of high frequency refractive index (n) of Ge ₁₅ Te _{85-x} Cu _x thin films	75
4.3.3. Analysis of refractive index (high frequency dielectric constant, ratio of carrier concentration (N/m [*]) and WDD model parameters for Ge ₁₅ Te _{85-x} Cu _x films	77
4.4. Interpretation of the physical properties of Ge ₁₅ Te _{85-x} Cu _x thin films and their dependence on energy	84
4.4.1. Average coordination number and the optical energy gap	86
4.4.2. Average heats of atomization and the optical energy gap	86
Chapter 5. Conclusions	89
Chapter 6. References	91

List of Table

- Table (3.1)** Composition of the prepared $\text{Ge}_{15}\text{Te}_{85-x}\text{Cu}_x$ amorphous samples.
- Table (4.1)** Optical band gap, β constant and Urbach energy E_t as a function of Cu content for $\text{Ge}_{15}\text{Te}_{85-x}\text{Cu}_x$ ($2 \leq x \leq 6 \text{ at. \%}$) thin films.
- Table (4.2)** The dielectric constant and the ratio N/m^* as a function of Cu content for $\text{Ge}_{15}\text{Te}_{85-x}\text{Cu}_x$ ($2 \leq x \leq 6 \text{ at. \%}$) thin films.
- Table (4.3)** Wemple–DiDomenico dispersion parameters (E_0 and E_d), E_0/E_g^{opt} ratio as a function of Cu content for $\text{Ge}_{15}\text{Te}_{85-x}\text{Cu}_x$ ($2 \leq x \leq 6 \text{ at. \%}$) thin films.
- Table (4.4)** The values of atomization energy H_s , coordination number $\langle r \rangle$ and the ratio $H_s/\langle r \rangle$ as a function of Cu content for $\text{Ge}_{15}\text{Te}_{85-x}\text{Cu}_x$ ($2 \leq x \leq 6 \text{ at. \%}$) thin films.

List of Figures

Figure (2.1)	Reflection, propagation and transmission of a light beam incident on an optical medium.	9
Figure (2.2)	Phenomena that can occur as a light beam propagates through an optical medium.	10
Figure (2.3)	Propagation of beam inside material of thickness dz	12
Figure (2.4)	The structural difference between amorphous and crystalline matter. To the left, a crystalline structure, with a periodic, long-range atomic ordering. the right, an amorphous structure, with no long-range atomic ordering.	13
Figure (2.5)	The ternary phase diagram shows the region of the glass formation in $\text{Ge}_{15}\text{Te}_{85-x}\text{Cu}_x$ with $(2 \leq x \leq 6 \text{ at.}\%).$	16
Figure (2.6)	Illustration of the electronic energy states, $E_{cc}, E_c, E_{ct}, E_{vt}, E_v$ and E_{vv} , in amorphous semiconductors. The shaded region represents the extended states. Energies E_c and E_{vv} correspond to the center of the conduction band and valence band extended states, and E_{ct} and E_{vt} represent the end of conduction band and valence band tail states, respectively.	18
Figure (2.7)	Typical spectral dependence of the optical absorption coefficient α in amorphous semiconductors.	20
Figure (2.8)	The mechanism of direct and indirect transitions in amorphous materials.	25
Figure (2.9)	Diagram of the interband direct transition process in a direct gap amorphous material.	27
Figure (2.10)	Diagram of the interband indirect transition process in an indirect gap amorphous material. The transition	29

must involve the absorption or emission of a phonon.

Figure (2.11)	Treatment of the indirect transitions in terms of direct transitions.	30
Figure (4.1)	The X-ray diffraction pattern for $\text{Ge}_{15}\text{Te}_{85-x}\text{Cu}_x$ thin films of compositions.	58
Figure (4.2)	Variation of absorption coefficient α with wavelength λ for $\text{Ge}_{15}\text{Te}_{85-x}\text{Cu}_x$ thin films of compositions..	60
Figure (4.3)	Variation of absorption coefficient α (cm^{-1}) with photon energy $h\nu$ for $\text{Ge}_{15}\text{Te}_{85-x}\text{Cu}_x$ thin films of compositions.	61
Figure (4.4)	Variation of extinction coefficient k with photon energy $h\nu$ for $\text{Ge}_{15}\text{Te}_{85-x}\text{Cu}_x$ thin films of compositions.	62
Figure (4.5)	Variation of k^2 with photon energy $h\nu$ for $\text{Ge}_{15}\text{Te}_{85-x}\text{Cu}_x$ thin films of compositions.	63
Figure (4.6)	Linear fitting of k^2 with photon energy $h\nu$ for $\text{Ge}_{15}\text{Te}_{85-x}\text{Cu}_x$ thin films of compositions.	64
Figure (4.7.a)	The relation between of $(k^2)^{1/2}$ versus $h\nu$ (eV) photon energy for $\text{Ge}_{15}\text{Te}_{83}\text{Cu}_2$ thin film.	65
Figure (4.7.b)	The relation between of $(k^2)^{1/2}$ versus $h\nu$ (eV) photon energy for $\text{Ge}_{15}\text{Te}_{82}\text{Cu}_3$ thin film.	65
Figure (4.7.c)	The relation between of $(k^2)^{1/2}$ versus $h\nu$ (eV) photon energy for $\text{Ge}_{15}\text{Te}_{81}\text{Cu}_4$ thin film.	66
Figure (4.7.d)	The relation between of $(k^2)^{1/2}$ versus $h\nu$ (eV) photon energy for $\text{Ge}_{15}\text{Te}_{80}\text{Cu}_5$ thin film.	66

Figure (4.7.e)	The relation between of $(\alpha h\nu)^{1/2}$ ($\text{cm}^{-1} \cdot \text{eV}$) ^{1/2} versus $\alpha h\nu$ photon energy for Ge ₁₅ Te ₇₉ Cu ₆ thin film.	67
Figure (4.8.a)	The dependence of $(\alpha h\nu)^2$ ($\text{cm}^{-1} \cdot \text{eV}$) ² on photon energy $\alpha h\nu$ for Ge ₁₅ Te ₈₃ Cu ₂ thin film.	68
Figure (4.8.b)	The dependence of $(\alpha h\nu)^2$ ($\text{cm}^{-1} \cdot \text{eV}$) ² on photon energy $\alpha h\nu$ for Ge ₁₅ Te ₈₃ Cu ₂ thin film.	68
Figure (4.8.c)	The dependence of $(\alpha h\nu)^2$ ($\text{cm}^{-1} \cdot \text{eV}$) ² on photon energy $\alpha h\nu$ for Ge ₁₅ Te ₈₂ Cu ₃ thin film.	68
Figure (4.8.d)	The dependence of $(\alpha h\nu)^2$ ($\text{cm}^{-1} \cdot \text{eV}$) ² on photon energy $\alpha h\nu$ for Ge ₁₅ Te ₈₁ Cu ₄ thin film.	68
Figure (4.8.e)	The dependence of $(\alpha h\nu)^2$ ($\text{cm}^{-1} \cdot \text{eV}$) ² on photon energy $\alpha h\nu$ for Ge ₁₅ Te ₈₀ Cu ₅ thin film.	69
Figure (4.9)	The dependence of $(\alpha h\nu)^2$ ($\text{cm}^{-1} \cdot \text{eV}$) ² on photon energy $\alpha h\nu$ for Ge ₁₅ Te ₇₉ Cu ₆ thin film.	69
Figure (4.9)	The dependence of $(\alpha h\nu)^2$ ($\text{cm}^{-1} \cdot \text{eV}$) ² on photon energy $\alpha h\nu$ for all five samples.	69
Figure(4.10)	The variation of energy optical gap with Cu content for Ge ₁₅ Te _{85-x} Cu _x thin films of compositions.	70
Figure(4.11)	Variation of refractive index with photon energy $\alpha h\nu$ for Ge ₁₅ Te _{85-x} Cu _x thin films of compositions.	73
Figure (4.12)	Variation of real part $(n^2 - k^2)$ of dielectric constant with wavelength λ (nm) for Ge ₁₅ Te _{85-x} Cu _x thin films of compositions.	75
Figure(4.13)	Variation of imaginary part $(2nk)$ of dielectric constant with wavelength λ (nm) for Ge ₁₅ Te _{85-x} Cu _x thin films of compositions.	75
Figure (4.14)	Variation of $n^2 - k^2$ with photon wavelength λ^2 (nm ²) for Ge ₁₅ Te _{85-x} Cu _x thin films of compositions.	76

Figure (4.15)	Linear fitting of n^2-k^2 with photon wavelength $\lambda^2(\text{nm}^2)$ for $\text{Ge}_{15}\text{Te}_{85-x}\text{Cu}_x$ thin films of compositions.	77
Figure (4.16)	Variation of refractive index factor with photon energy $(h\nu)^2$ (eV) ² for $\text{Ge}_{15}\text{Te}_{85-x}\text{Cu}_x$ thin films of compositions.	79
Figure (4.17)	Linear fitting of refractive index factor with photon energy $(h\nu)^2$ (eV) ² for $\text{Ge}_{15}\text{Te}_{85-x}\text{Cu}_x$ thin films of compositions.	79
Figure (4.18)	Variation of Wemple-DiDomenico parameters as a function of Cu content for $\text{Ge}_{15}\text{Te}_{85-x}\text{Cu}_x$ thin films of compositions.	81
Figure (4.19)	Variation of average coordination number $\langle \mu \rangle$ with Cu content for $\text{Ge}_{15}\text{Te}_{85-x}\text{Cu}_x$ thin films of compositions	83
Figure (4.20)	Optical energy gap E_g and the average heat of atomization per single bond $H_a/\langle \mu \rangle$ as a function of the average coordination number for $\text{Ge}_{15}\text{Te}_{85-x}\text{Cu}_x$ thin films of compositions.	85

Interest in the physical properties of amorphous chalcogenide glasses and other noncrystalline materials, especially their potential applications in areas of optoelectronics such as laser technology and fiber optics, has gained attention since the 1950's and has coalesced within a field known academically as "Physics of Noncrystalline Solids". However, in contrast to crystalline solids, for which the physical properties and structures are essentially understood, there remain considerable theoretical difficulties with amorphous solids, and these have been amplified by a lack of precise, organized experimental information. Consequently, relative newcomers to this field generally must piece together information from many sources especially experimental results [1]. It is the purpose of this study to contribute to this field, studying optical properties of amorphous chalcogenide thin films.

The absence of long-range periodic constraints in amorphous semiconductors compared to their crystalline counterparts facilitates the preparation of these glasses in varied compositions. The variation in composition brings changes in short-range order resulting variation in physical properties, which help in tailoring the properties of these materials to a desired requirement [2].

Chalcogenide glasses like germanium-tellurium (Ge-Te) are known to be very good covalently bonded glass formers. The dominant feature of the network is four-fold coordinated Ge. The structure of these glasses is a function of composition. Studies of the optical properties of tellurium (Te) based chalcogenide glasses have attracted several workers as these

materials possess wide range of applications in solid state devices both in scientific and technological fields [3].

In addition Ge-Te chalcogenide materials show an appreciable optical change between their amorphous and crystalline states. Electronic transitions in Ge-based chalcogenide films are particularly of interest for reversible optical data storage due to their structure-dependent optical properties [4].

Also chalcogenide semiconductors have shown interesting electrical effects involving a sudden change in resistance, they are grouped as switching properties. In a chalcogenide glass memory device, the memory action is the result of a reversible structural change between an amorphous state, which is of high resistance, and a small-grain crystalline state, which is of low resistance [5].

The doping effect of chalcogenide glasses semiconductors with metal is an effective step of controlling the optical properties. The metal atoms are tetrahedrally coordinated and the general structural model proposed by Liang and Taylor [6,7] assumes a tetrahedral structure when copper (Cu) is added to glasses.

Therefore, we have studied the effect of copper (Cu) into the $\text{Ge}_{15}\text{Te}_{85}$ (germanium-tellurium) binary system at the expense of the Te content. As shown in this study, addition of a third element expands the glass-forming area and also creates compositional and configurational disorder in the system. The lattice perfection and the energy band gap of the material play

a major role in the preparation of the device for a particular wavelength, which can be modified by the addition of dopants as E. Marquez et al. reported [6]. So, the influence of additives on the properties has been an important issue in the case of chalcogenide glasses. Instead of providing a localized impurity level in the mobility gap, the additives may merely

alter the mobility of the charge carriers or may introduce structural changes in the amorphous materials with or without modification of the localized states in the forbidden gap [7].

Chalcogenide glasses [8] are produced by melting together Group **16** ‘chalcogen elements’, viz., S, Se, and Te with other elements, generally of Group **15** (e.g. Ge, Si) to form covalently bonded solids. When melted in an atmosphere particularly deficient in oxygen and water, the glasses have unique optical and semiconducting properties. Specifications of amorphous chalcogenide glasses have been discussed briefly in chapter 2.

In contrast to crystalline semiconductors [8], chalcogenide amorphous semiconductors have high refractive index (n) higher than 2, a convenient optical gap (E_g^{opt}) ($E_g^{\text{opt}} \sim 1.48 - 1.69 \text{ eV}$), for samples in this study which causes them to be essentially opaque through the visible spectrum to begin transmission around $1 \mu\text{m}$, possibly to $2 \mu\text{m}$ (mid-IR).

By optical properties of solids, we mean those properties that relate to the interaction of solids with electromagnetic radiation whose wavelength is in the infrared to the ultraviolet. There are several aspects to optical properties of solids and looking at the subject in full generality can often lead to complexity, whereas treating each part as a separate case often leads to confusion. We will try to keep to a middle ground between these, by emphasizing only one topic (absorption) but treating it in some detail [9].

A reasonable knowledge of optical absorption edge has been briefly discussed in this study, where the optical absorption spectra was related to the band structure (optical energy gap) in terms of Tauc's relation [10] for high absorption regions and Urbach's relation [11] for low absorption regions, as mentioned in section (2.4.2). A general feature of optical

absorption phenomena process was represented and discussed in terms of electronic transitions in section (2.4.3).

The process of relating measured optical phenomena to the electronic and optical properties of the material under study can proceed in two ways. We can work forwards from known electronic and optical physics to predict the results of optical experiments, or we can work backwards from experimental data to microscopic properties, the second procedure was applied in this study.

Five $\text{Ge}_{15}\text{Te}_{85-x}\text{Cu}_x$ ($2 \leq x \leq 6, \text{at.}\%$) thin films prepared by thermal evaporation using raw high purity elements (99.999%) in appropriate proportions, the optical absorption and transmission data were obtained using a double beam spectrophotometer in wavelength range 280-1000 nm with 5 nm steps, experimental techniques were presented in details in chapter (3).

Optical parameters of Ge-Te thin films have been studied by analyzing the transmission spectra. This analysis was pioneered by J.C. Manifacier et al.[12] and extended by Swanepoel [13] and since then it has successfully been applied to several chalcogenide glasses. In this study the straightforward analysis proposed by Swanepoel has been successfully employed, and it has allowed us to determine optical constants.

Tauc's relation for allowed direct transition describes the optical transition in the studied films. The optical constants determined were optical band

gap E_g^{opt} , absorption coefficient (α), refractive index (n), and extinction coefficient (k), analysis of refractive index has yielded to real and imaginary parts of the complex dielectric constant (ϵ_∞), the ratio of carrier concentration (N/m^*) and more other constants. The variation of

these constants with photon energy was reported. The optical band gap has been calculated using Tauc's extrapolation method. A relationship between Cu content and the E_g^{opt} has been established.

The dispersion of refractive index has been studied in terms of the Wemple-DiDomenico [14,15] single oscillator model, by using this model dispersion parameters were determined and related to the optical energy gap.

The obtained results were correlated with the character of the chemical bond for the prepared compositions through a study of parameters such as the average coordination number $\langle r \rangle$ and the average heat of atomization H_s , these two parameters were correlated to the optical energy gap in section (4.3).

Results were explained in terms of Bond Constraint Theory (BCT) and Rigidity Theory.

This dissertation contains six chapters as following

Chapter 1: Introduction.

Chapter 2: Theoretical Considerations and Literature Survey.

Chapter 3: Experimental Techniques.

Chapter 4 : Results and Discussions obtained in this study.

Chapter 5 : Conclusions.

Chapter 6 : References.

2.1. Introduction

The optical properties of chalcogenide glasses, for example its excellent transmittance in the infra-red region, the continuous shift of the optical absorption edge, the high values of refractive index n , as well as the strong correlation between the former properties and the chemical composition explain the growing interest in these semiconducting materials for the manufacture of filters, anti-reflection coatings, and a wide range of optical devices. This underlines the importance of the characterization of these glassy materials through the determination of their optical constants, refractive index n and extinction coefficient k , as well as the corresponding optical band gaps [17-19].

2.2. Classification of optical processes

The wide-ranging optical properties observed in solid state materials can be classified into a small number of general phenomena. The simplest group, namely reflection, propagation and transmission, is illustrated in figure (2.1). This shows a light beam incident on an optical medium. Some of the light is reflected from the front and back surfaces and also to the way the light propagates through the medium.

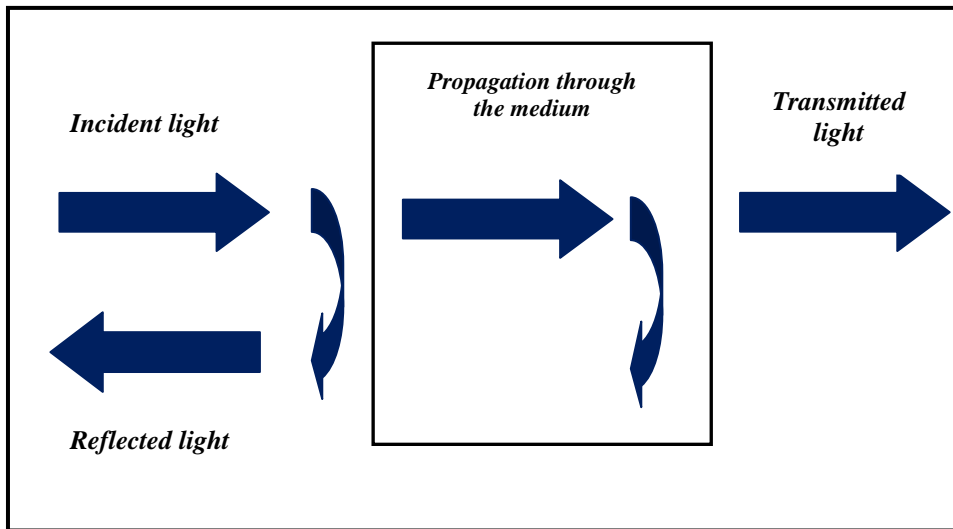


Fig. (2.1) Reflection, propagation and transmission of a light beam incident on an optical medium.

The phenomena that occur while light propagates through an optical medium are illustrated schematically in figure (2.2). Refraction causes the light waves to propagate with a smaller velocity than in free space. This reduction of the velocity leads to the bending of light rays interfaces described by Snell's law of refraction. Refraction, itself, does not affect the intensity of the light wave as it propagates.

Absorption occurs during the propagation if the frequency of the light is resonant with the transition frequencies of the atoms in the medium. In this case, the beam will be attenuated as it progresses. The transmission of the medium is clearly related to the absorption, because only unabsorbed light will be transmitted [20].

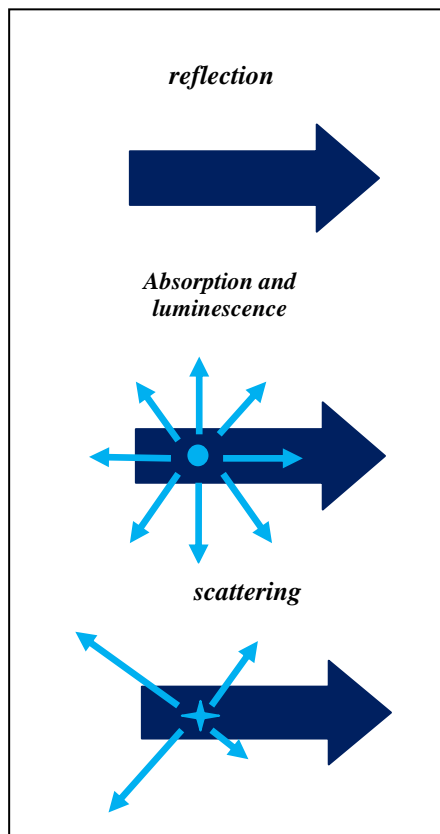


Fig. (2.2) *Phenomena that can occur as a light beam propagates through an optical medium.*

Luminescence is the general name given to the process of spontaneous emission of light by excited atoms in a solid state material. The atom jumps to an excited state by absorbing a photon, then relaxes to an intermediate state, and finally re-emits a photon as it drops back to ground state.

Scattering is the phenomenon in which the light changes direction and possibly also its frequency after interacting with the medium. The total number of photons is unchanged, but the number going in the forward direction decreases because light is being re-directed in other directions. Scattering therefore has the same attenuating effect as absorption.

The optical phenomena described previously can be quantified by a number of parameters that determine the properties of the medium at the macroscopic level.

The reflection at the surface is described by the coefficient of reflection or reflectivity. This is usually given the symbol R and is defined as the ratio of the reflected power to the power incident on the surface. The coefficient of transmission or transmittivity T is defined likewise as the ratio of the transmitted power to the incident power. If there is no absorption or scattering, then by conservation of energy we must have

$$R + T = 1 \quad (2.1)$$

The propagation of the beam through a transparent medium is described by the refractive index n . This is defined as the ratio of the velocity of light in free space c to the velocity of light in the medium v according to

$$n = \frac{c}{v} \quad (2.2)$$

the refractive index depends on the frequency of the light. This effect is called dispersion, and will be discussed later on.

The absorption of light by an optical medium is quantified by its absorption coefficient (α) in cm^{-1} . This is defined as the fraction of the power absorbed in a unit length of the medium. If the beam is propagating in the z direction, and the intensity (optical power per unit area) at position z is $I(z)$ see Fig (2.3), then the decrease of the intensity in an incremental slice of thickness dz is given by

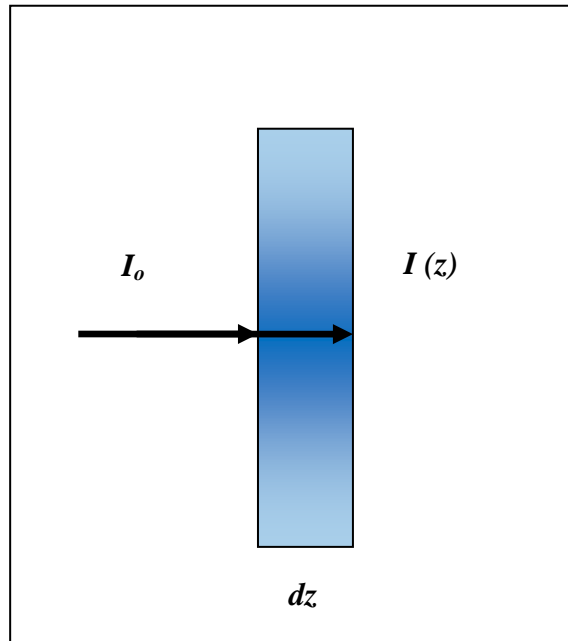


Fig. (2.3) Propagation of beam inside material of thickness dz

$$dI = -\alpha dz \times I(z) \quad (2.3)$$

Integrating the past equation gives us Beer's Law [21]

$$I(z) = I_0 e^{-\alpha z} \quad (2.4)$$

where I_0 is the optical intensity at $z=0$ [20].

2.3. Amorphous chalcogenide glasses

Optical materials can be loosely classified into five categories [20]

- Crystalline insulators and semiconductors
- Glasses
- Metals
- Molecular materials
- Doped glasses and insulators.

In this study we focused on doped glass materials and in specific amorphous chalcogenide glasses doped with metal.

2.3.1. Specifications of amorphous chalcogenide glasses

Amorphous state is the state of solid that has become disordered. Most solid materials can be found or prepared in an amorphous form. For instance, common window glass is an amorphous solid, many polymers (such as polystyrene) are amorphous, and even foods such as cotton candy are amorphous solids. The main feature of the structure of matter in the amorphous state is the absence of long-range order which is clearly seen in crystalline materials, figure (2.4). The amorphous state has short-range order within the limits of one or several unit cells. Each unit cell differs from the preceding in its position in space.

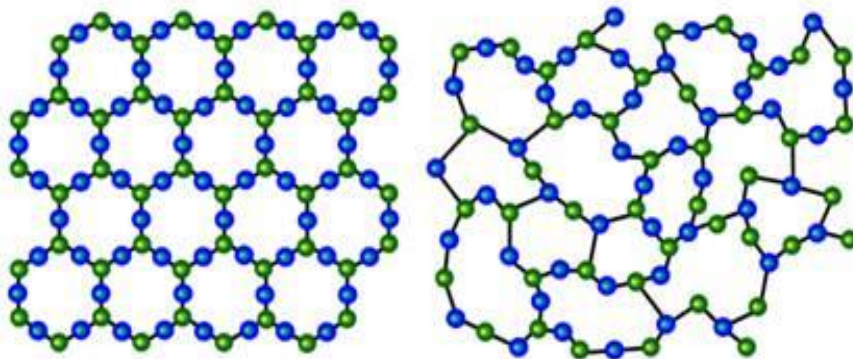


Fig. (2.4) The structural difference between amorphous and crystalline matter. To the left, a crystalline structure, with a periodic, long-range atomic ordering. the right, an amorphous structure, with no long-range atomic ordering.

Amorphous semiconductors can be prepared as thin films by evaporation or sputtering, or in some materials as bulk glasses by super cooling the melt. In principle, given a sufficiently high cooling rate, any liquid can be made into an amorphous solid. Cooling reduces molecular mobility. If the cooling rate is faster than the rate at which molecules can organize into a more thermodynamically favorable crystalline state, then an amorphous solid will be formed. Because of entropy considerations, many polymers can be made amorphous solids by cooling even at slow rates. In contrast, if molecules have sufficient time to organize into a structure with two- or three-dimensional order, then a crystalline (or semi-crystalline) solid will be formed. Water is one example, because of its small molecular size and ability to quickly rearrange, it cannot be made amorphous without resorting to specialized hyper quenching techniques.

Two distinct classes of amorphous semiconductors are widely studied: tetrahedral-bonded amorphous solids such as silicon and germanium, and the chalcogenide glasses. The latter are multi-component solids of which one major constituent is a "chalcogen" element (sulfur, selenium, or tellurium). The tetrahedrally-bonded materials have properties similar to those of their crystalline forms. They can be doped with small amounts of chemical impurities, and their conductivity can be sharply modified by injection of free carriers from a metallic contact [22].

Chalcogenide glasses are a recognized group of inorganic glassy materials. They are produced by melting together Group **16** (chalcogen elements), viz., tellurium (Te), selenium (Se), and sulphur (S) with other elements, generally of Group **15** (e.g. antimony (Sb), arsenic (As) or Group **14** (e.g. germanium (Ge), silicon (Si)) to form covalently bonded solids. In contrast to silicate glasses, the chalcogenide have a semiconductor type band gap (1-3 eV) which causes them to be essentially opaque through the visible spectrum. In addition, chalcogenide

containing materials are very appropriate materials for optical memories because amorphous or crystalline state is reachable due to high structural flexibility [9].

Additionally, the absence of long-range order allows modification of their properties to a specific technological application by continuously changing their chemical composition. Hence, the study of the dependence on composition of their properties is of great importance to improve the understanding of the mechanisms underlying these phenomena and also to improve their applications in technology [23].

2.3.2. Structure study of amorphous chalcogenide semiconductors (Ge-Te-Cu alloy)

Determination of the structure of a crystalline solid is made straightforward by the need only to solve the structure within the unit cell, containing relatively few atoms in most cases which represents the fundamental building unit of the structure. The structure of the crystal as a whole is then generated by repeating in a periodic fashion the position of the unit cell in space.

Such a procedure is impossible for a non periodic amorphous solid, for which the unit cell may be regarded as being infinite extent.

Germanium tellurium alloy Ge-Te has low glass-formation ability. Glasses of the binary system Ge-Te are obtained in a limited range of compositions and only when the melt is quenched. With increasing the number of components in the alloys based on Ge-Te (e.g. the system germanium-tellurium-copper Ge-Te-Cu) it's ability to form glasses is increased because of the more complicated composition of the melt. The chosen compositions of Ge-Te-Cu were belonging to the vitreous region determined in (Fig.2.5).

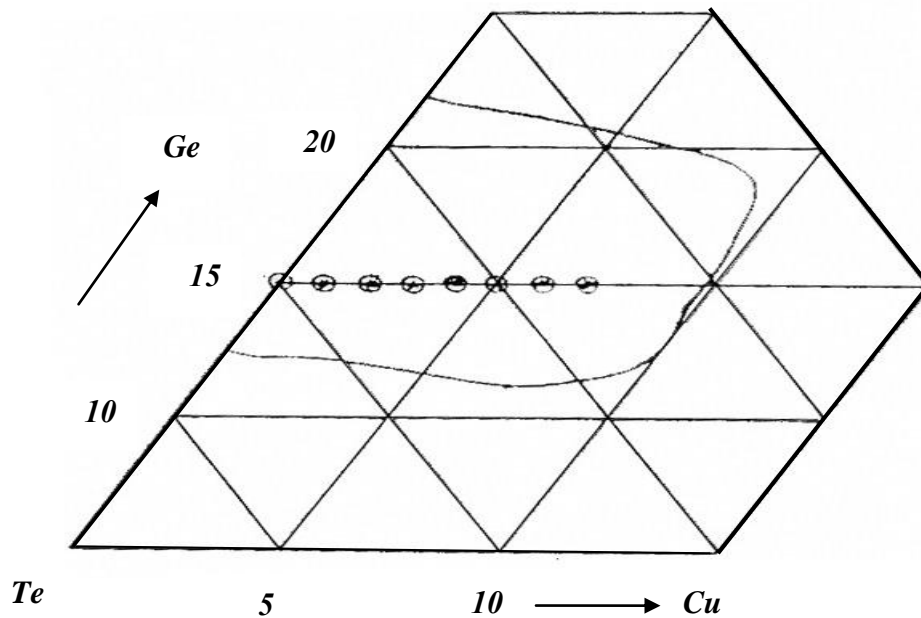


Fig.(2.5) The ternary phase diagram shows the region of the glass formation in $Ge_{15}Te_{85-x}Cu_x$ with $(2 \leq x \leq 6 \text{ at. \%})$.

2.4. Optical Properties

2.4.1. Specifications of energy gap in amorphous semiconductors

In a defect-free crystalline semiconductor, there exists a well defined energy gap between the valence and conduction bands. In contrast, in an amorphous semiconductor, the distributions of conduction- and valence-band electronic states do not terminate abruptly at the band edges. Instead, some of the electronic states, referred to as tail states, encroach into the otherwise empty gap region [24].

In addition to tail states, there are other localized states deep within the gap region. These localized tail states in amorphous semiconductors arise as a consequence of defects. The defects in amorphous semiconductors are considered to be all cases of departure from the normal nearest-neighbor coordination (or normal valence requirement). Examples of defects are broken and dangling bonds (typical for amorphous silicon), over- and under-coordinated atoms (such as ‘valence alternation pairs’ in chalcogenide glasses), voids, pores, cracks, and other macroscopic defects [25].

As these tail and deep defect states are localized, and there exist mobility edges, which separate these localized states from their extended counterparts [26,27]. These localized tail and deep defect states are responsible for many of the unique properties exhibited by amorphous semiconductors. A representation of the current understanding of the distribution of electronic states, for the case of amorphous Si-H, is schematically presented in figure (2.6) [28,29].

Despite years of intensive investigation, the exact form of the distribution of electronic states associated with amorphous semiconductors remains a matter for debate. While there are still some unresolved issues, there is general consensus that the tail states arise as a consequence of the disorder (weak and dangling bonds) present within the amorphous network, and that the breadth of these tails reflects the amount of disorder present. The existence of tail states in amorphous solids has a profound impact upon the band-to band optical absorption [30].

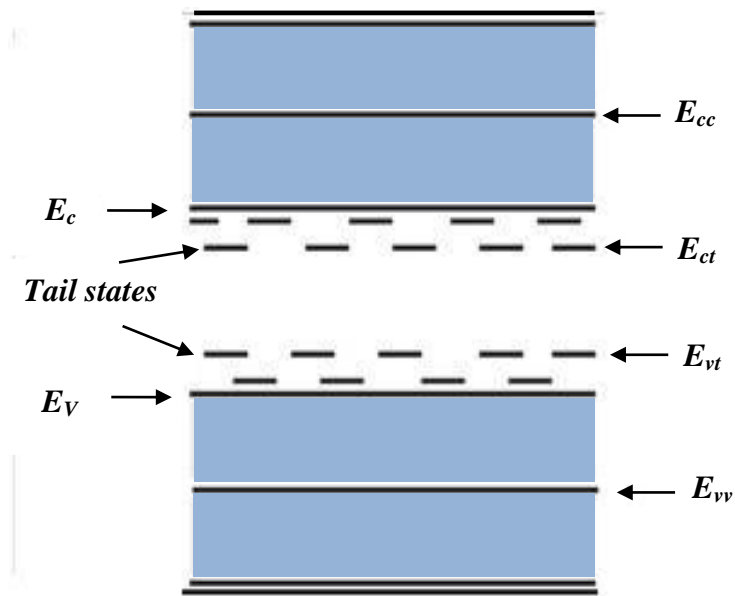


Fig. (2.6) Illustration of the electronic energy states, E_{cc} , E_c , E_{ct} , E_{vt} , E_v and E_{vv} , in amorphous semiconductors. The shaded region represents the extended states. Energies E_{cc} and E_{vv} correspond to the center of the conduction band and valence band extended states, and E_{ct} and E_{vt} represent the end of conduction band and valence band tail states,

Unlike the case of a crystalline solid, the absorption of photons in an intrinsic amorphous solid can also occur for photon energies below the optical gap, i.e., $h\nu \leq E_g^{opt}$, due to the presence of the tail states in the forbidden gap, E_g^{opt} denoting the optical gap (i.e. the energy difference between the conducting and the valence mobility edges), which is usually close to the mobility gap, i.e., the energy difference between the conduction- and valence-band mobility edges [31].

2.4.2. Optical absorption edge

Absorption edge is caused by the onset of optical transitions across the fundamental band gap of the material. The process that occurs when electrons are excited between the bands by making optical transitions is called interband absorption. The understanding of interband absorption is based on understanding of the light-matter interaction [19].

Analysis of the optical absorption spectra is one of the most useful tools for understanding the electronic structure of solids in any form, crystalline or amorphous. Applying this to amorphous structures with the first approach leads to the well known Tauc's plot for the optical absorption coefficient α (which determines the optical energy gap) as a function of photon energy $h\nu$, giving: $(\alpha h\nu)^{1/2} \propto (h\nu - E_g^{opt})$ [32].

In the absorption process, a photon of known energy excites an electron from a lower to a higher energy state, corresponding to an absorption edge. In chalcogenide glasses, a typical absorption edge can be ascribed to either of three processes [33]:

- (1) Residual below-gap absorption
- (2) The Urbach tails
- (3) Interband absorption

Chalcogenide glasses have been found to exhibit highly reproducible optical edges, which are relatively insensitive to preparation conditions and only the observable absorption with a gap under equilibrium conditions account for the process (1). In the second process the

absorption edge depends exponentially on the photon energy according to the Urbach relation (discussed later on).

In crystalline materials, the fundamental edge is directly related to the conduction and valance band, i.e. direct and indirect band gaps, while in the case of amorphous a different type of optical absorption edge is observed [34].

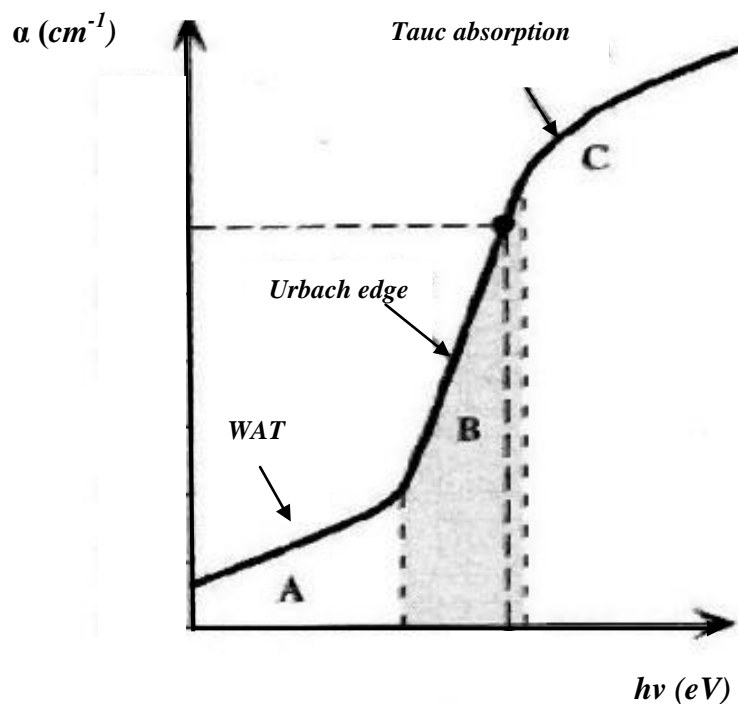


Fig. (2.7) Typical spectral dependence of the optical absorption coefficient α in amorphous semiconductors.

According to Tauc [11] it is possible to isolate three distinct regions in the absorption edge spectrum in amorphous semiconductors. The shape of the absorption curve is shown in figure (2.7).

One can distinguish the high absorption region, **C**, ($\alpha > 10^4 \text{ cm}^{-1}$) where α is the absorption coefficient, the exponential region, **B**, which is strongly related to the structure randomness of the system, and the weak absorption tail region **A**, which originates from defects and impurities.

In **A** and **B** regions, the optical absorption is controlled by the optical transitions between tail to tail, and tail to extended states, respectively, and in **C** region it is dominated by transitions from extended to extended states [35].

2.4.2.1. High Absorption region

In the case of amorphous semiconductors, the optical absorption coefficient, in the high absorption region ($\alpha > 10^3 \text{ cm}^{-1}$) (region **C** in figure (2.7)), is given according to Tauc [11] by the following equation:

$$(\alpha h\nu) = \beta(h\nu - E_g^{opt})^r \quad (2.5)$$

where E_g^{opt} is the optical band gap, $h\nu$ is the incident photon energy, α is the absorption coefficient, β is a constant which depends on the transition probability and r is a parameter which characterizes the optical

absorption process and depends on the type of electronic transition responsible for the absorption, and has values of $1/2$, $3/2$, 2 and 3 , where

$r = 1/2$ for a direct allowed transition, $r = 3/2$ for direct forbidden transition, $r = 2$ for an allowed indirect transition and $r = 3$ for an indirect forbidden transition [36].

The defined optical gap E_g^{opt} is called the Tauc gap. It is conveniently determined from the so-called Tauc plot. The Tauc gap is often applied in practice to characterize the optical properties of amorphous materials. The optical energy gap of the amorphous material plays a major role in

the preparation of the device for a particular wavelength, which can be modified by the addition of impurity [37].

In amorphous solids it is quite possible that even in the ‘forbidden’ zone, there exists a finite density of localized states. For that reason, the terminus “optical gap” is not well defined for amorphous semiconductors. On the other hand, the introduction of the optical gap by a dependence like equation (2.5) gives at least a recipe for unambiguous and convenient determination of a parameter that may be used to judge the quality of a prepared material with respect to certain optical applications. For that reason, these parameters are widely used in applied semiconductor research.

2.4.2.2. The exponential region of the absorption edge (Urbach edge)

In the exponential region part **B** in figure (2.7), where ($\alpha < 10^3 \text{ cm}^{-1}$) the absorption coefficient can be described by the following relation, Urbach's relation [12]

$$\alpha(\nu) = \alpha_0 \exp\left(\frac{h\nu}{E_t}\right) \quad (2.6)$$

where ν is the frequency of the radiation, h is Planck's constant, α_0 is a material dependent constant and E_t is the Urbach energy (related to the width of the band tail of the localized states in the gap region and in general represents the degree of disorder in an amorphous semiconductor).

The value of E_t lies between 0.05 eV and 0.08 eV in many semiconductor glasses and varies slightly with composition. The value of E_t can be calculated using Urbach's empirical relation [38]

$$\ln(\alpha) = \ln(\alpha_0) - \left(\frac{h\nu}{E_t}\right) \quad (2.7)$$

The absorption in this region is due to transitions between extended states in one band and localized states in the exponential tail of the other band. The origin of the exponential dependence of the absorption coefficient on the energy in amorphous semiconductors is not clearly known. Dow and Redfield [39] suggested that it might arise from random fluctuations of the internal field associated with the structural disorder in amorphous solids. Zanini and Tauc [40] believe that the value of E_t arises from electronic transitions on localized states where the density of the localized states exponentially depends on the energy. Davis and Mott [41] reported that this explanation is not valid for all disordered materials because the slope of observed exponential behavior remains unchanged for many crystalline and non-crystalline materials.

2.4.2.3. Weak absorption tail region (WAT)

In this region, (region **A**), ($\alpha < 1 \text{ cm}^{-1}$) see figure (2.7), the absorption of photons of energy less than the optical band gap energy, $E_g^{opt} \geq h\nu$, involves the localized tail states and hence follows neither equation (2.5) nor equation (2.6). The optical absorption in this region is characterized by optical transitions from transitions between tail-to-tail states. The localized tail states in amorphous semiconductors arise from defects [31].

2.4.3. Absorption Process (direct and indirect transitions)

The fundamental absorption takes place when one electron is excited by absorption of a photon. There are two types of transitions that must be distinguished, see figure (2.8):

- 1- **direct transition** in which only a photon is involved.
- 2- **indirect transition** in which one or more phonons are emitted or absorbed at the same time as the photon is absorbed.

So, it must be distinguished between two types of semiconductors, since their behavior is rather different.

The first type consists of those semiconductor, for which the wave vector (K) for the lowest energy state in the conduction band, as for the highest energy state in the valance band i.e. $K = 0$ (direct transition).

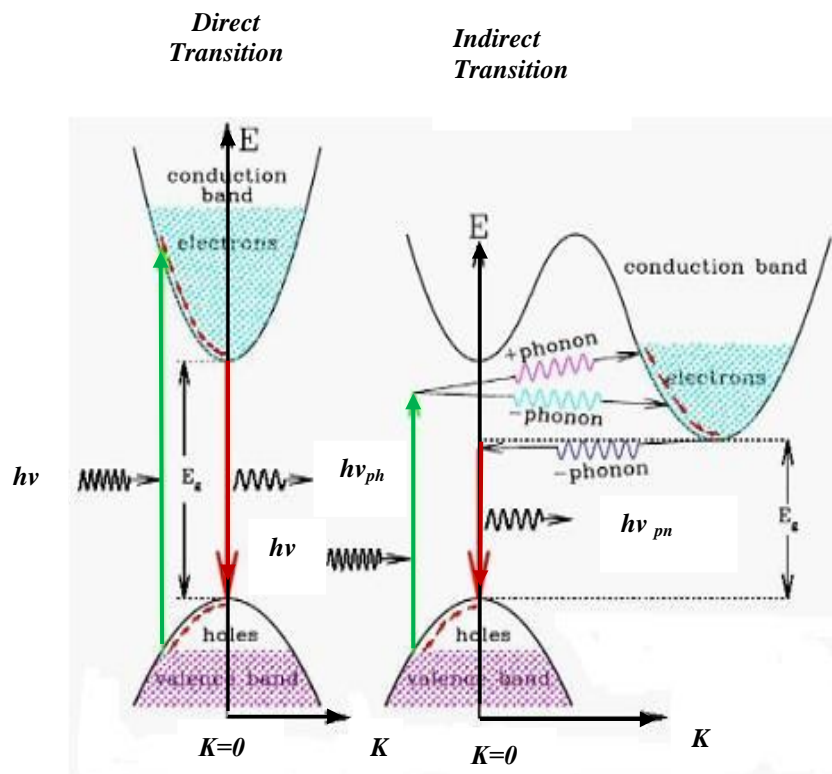


Fig. (2.8) The mechanism of direct and indirect transitions in amorphous materials

The second type consists of those semiconductor, for which the band edges of the conduction and valance bands are widely separated in K space. For example Si and Ge are typical of the $K \neq 0$ usually indirect transition.

When the semiconductor becomes amorphous, it could be observed, a shift

of the absorption edge either towards lower or higher energies. The shape of the absorption curve appears to be similar for many amorphous semiconductors [20].

2.4.3.1. Direct transition

Electronic optical absorption processes are called direct transition if only an optical photon is involved in the process, producing negligible change in the wave vector of the electron.

A direct optical transition involving the absorption of a photon only with creation of an electron and a hole, with no phonon involved. The energy of a photon absorbed must be equal to the band gap energy for a transition from the top of the valance band to the bottom of the conduction band, and there is almost no change in K upon making the transition.

The direct transition is shown in figure (2.9). If the limits of the energy bands plotted against the wave vector K , the conduction band minimum and valance band maximum occur at $K = 0$, then the absorption edge makes well.

In figure (2.9) only vertical transitions are allowed. Non-vertical transitions

are normally forbidden. In practice this does not mean that the latter do not occur at all, but only that absorption due to such transitions is of much lower intensity [20].

Thus a plot of the absorption coefficient squared versus photon energy, for a direct band gap, should be linear for energies above the fundamental transition. The intercept as the value of the optical band gap. The factor β could be determined from the slope of the same plot.

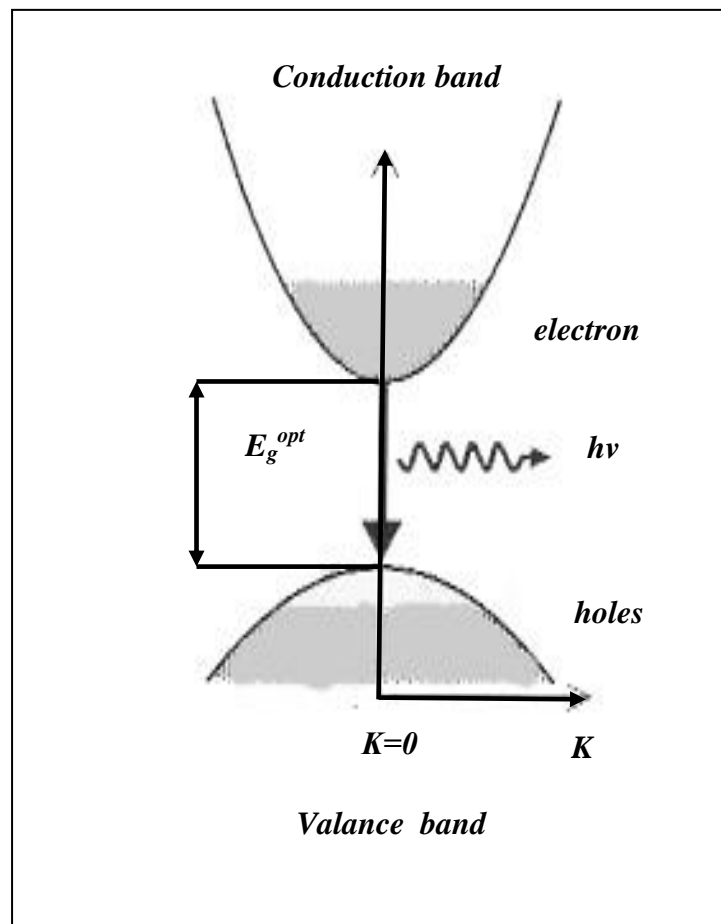


Fig.(2.9) *Diagram of the interband direct transition process in a direct gap amorphous material.*

2.4.3.2. Indirect transition

This is the reverse of the indirect absorption process. In an indirect gap material, the conduction band minimum and valence band maximum are at different points in the Brillouin zone. Indirect transitions can be thought of as a two step process: (1) the absorption of a photon ($h\nu$) and (2) emission or absorption of a phonon. Figure (2.10) shows the $E - \mathbf{K}$ diagram of an indirect transition, the conduction band minimum does not occur at $\mathbf{K} = 0$, but rather at some other value of \mathbf{K} . Both photon absorption and emission and absorption of phonons are considered. In fact in many cases, it is even necessary to consider the emission and/or absorption of several phonons for a single transition [20]. An indirect optical transition involving the absorption of a photon and either the absorption or the emission of a phonon is pictured in figure (2.10). Conservation of energy and wave vector under this condition requires

$$E_{ph} \pm E_{pn} = E_g^{opt} \quad \Delta E = \mathbf{K}_{pn} \quad (2.8)$$

where E_{ph} and E_{pn} and \mathbf{K}_{pn} represent the energy of photon, the energy of emission or absorbed phonon and the wave vector of phonon respectively.

The indirect transition takes place in two ways. Firstly, an electron may be excited without change in wave vector \mathbf{K} from near the top of the valence band, $\mathbf{K} = 0$, and leave a hole with $\mathbf{K} = 0$. The first transition is a vertical direct transition from the initial state 0 to a state of the same value \mathbf{K} in the conduction band [**transition (1)**] as shown in figure (2.11).

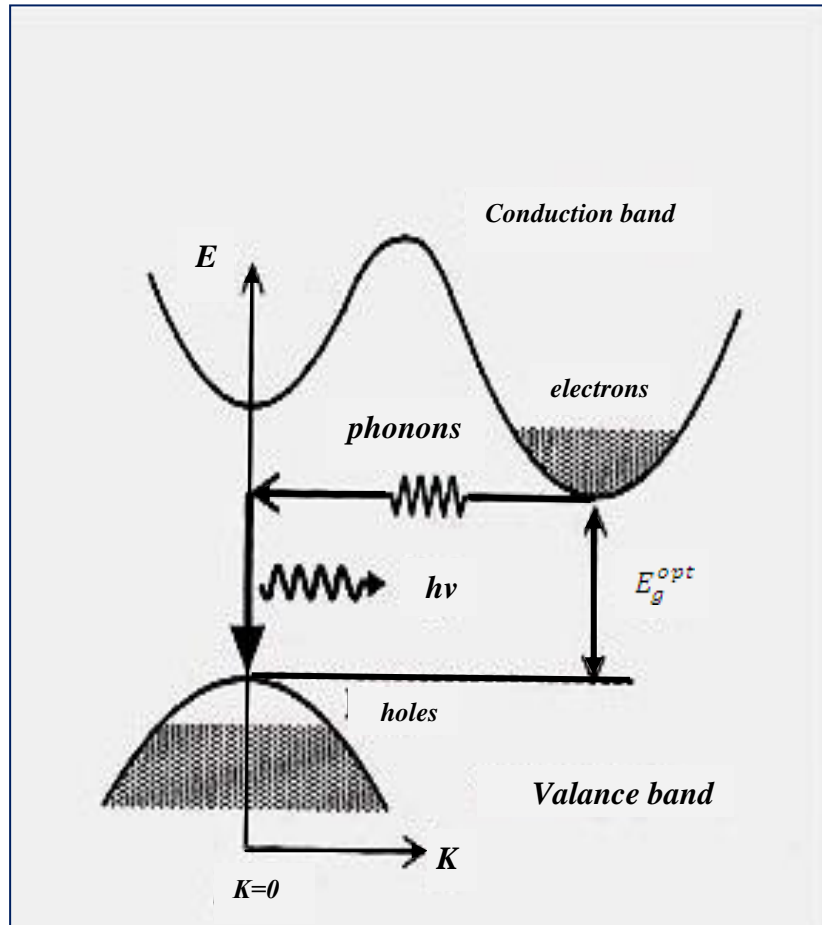


Fig. (2.10) *Diagram of the interband indirect transition process in an indirect gap amorphous material. The transition must involve the absorption or emission of a phonon.*

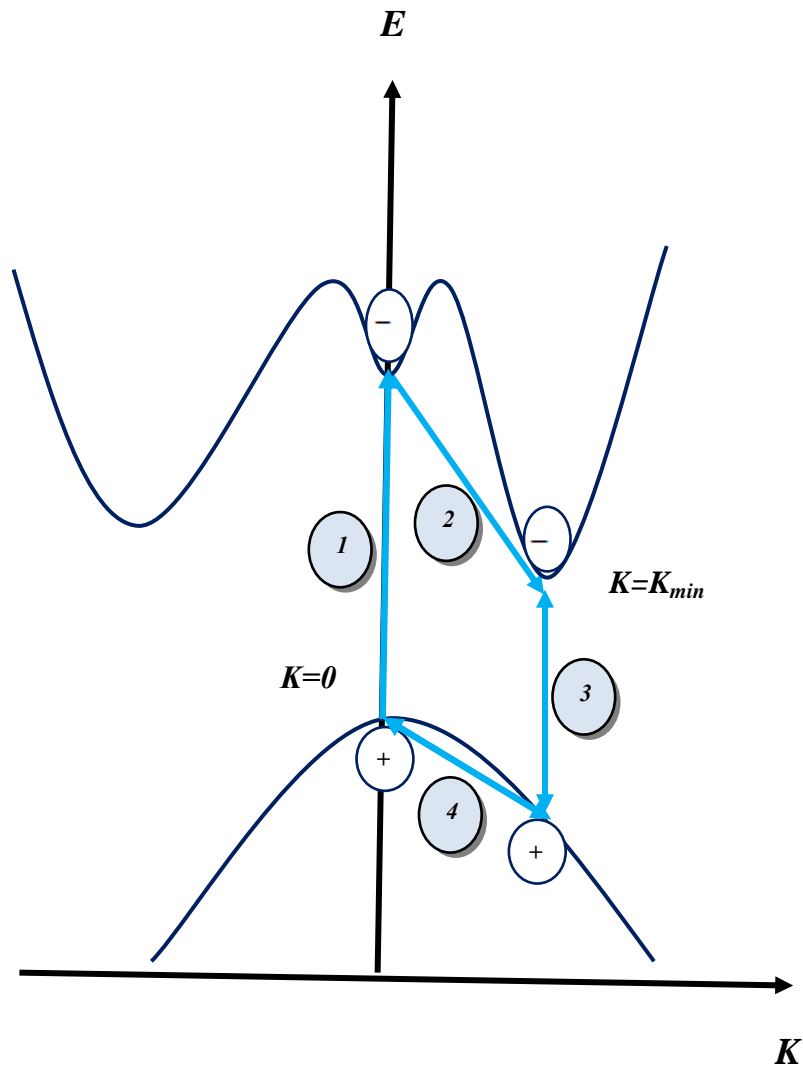


Fig. (2.11) *Treatment of the indirect transitions in terms of direct transitions.*

Since this state has higher energy than the minimum of the band, then the electron quickly makes a phonon-assisted transition to a state with energy near the minimum energy of the band with emission or absorption of a phonon of momentum equal to K_{min} [transition (2)], see figure (2.11). Secondly, an electron may be excited vertically from deep level in the valance band to a state having a value of K equal K_{min} . This electron leaves a positive hole deep in the valance band [transition (3)]. This hole then makes a transition to a state with energy near the maximum energy of the valance band (with $K = 0$), with emission or absorption of a phonon [transition (4)].

2.5. Optical constants

Optical properties of a material change or effect the characteristics of light passing through it by modifying its propagation vector or intensity. Two of the most important optical properties are the refractive index \mathbf{n} and the extinction coefficient \mathbf{k} , which are generally called **optical constants**; through some authors include other optical coefficients within this terminology. The latter is related to the attenuation or absorption coefficient α . In this section we present the refractive index, the frequency or wavelength dependence of \mathbf{n} and, \mathbf{k} so-called dispersion relations, how \mathbf{n} and \mathbf{k} can be determined by studying the transmission as a function of wavelength through a thin film of the material.

One of the most important optical constants of a material is its refractive index, which in general depends on the wavelength of the electromagnetic wave, through a relationship called dispersion. In materials where an electromagnetic wave can lose its energy during its propagation, the refractive index becomes complex. The real part is usually the refractive index, n , and the imaginary part is called extinction coefficient, \mathbf{k} [31].

2.5.1. The refractive index (n), extinction coefficient (k) and real and imaginary parts of high frequency dielectric constant

If multiple reflections are neglected, the transmissivity T of an absorbing medium of thickness d is given [20] as:

$$T = (1 - R_1)\exp(-\alpha d)(1 - R_2) \quad (2.9.a)$$

Where R_1 and R_2 are the reflectivities of the front and back surfaces respectively. This equation applies to the transmission of light through an optical medium such as the one shown in figure (2.1). The first and third terms on the right hand side of equation (2.9.a) account for the transmission of the front and back surfaces respectively, while the middle term gives the exponential decrease in intensity due to the absorption according Beer's law (see eq. (2.4)). If the front and back surfaces have equal reflectivities R , as will usually be the case, then equation (2.9.a) simplifies to

$$T = (1 - R)^2 \exp(-A) \quad (2.9.b)$$

where $A = \alpha d$, the reflection of the specimen can be determined from measurements of both the transmission and absorption using equation (2.9.b).

The relationship between α and k can be described by considering the propagation of plane electromagnetic waves through a medium with a complex refractive index. If the wave is propagating in the z -direction, the spatial and time-dependence of the electric field is given by

$$E(z, t) = E_0 e^{i(Kz - \omega t)} \quad (2.10)$$

Where \mathbf{K} is the wave vector ($\bar{\mathbf{K}} \cdot \bar{\mathbf{r}} = Kz$), of the electromagnetic light and ω is the angular frequency, $|E_0|$ is the amplitude at $z = 0$. In a non-absorbing medium of refractive index n , the wavelength of the light is reduced by a factor n compared to the free space wavelength λ , k and ω are therefore related to each other through

$$k = \frac{2\pi}{(\lambda/n)} = \frac{n\omega}{c} \quad (2.11)$$

This can be generalized to the case of an absorbing medium by allowing the refractive index to be complex

$$k = \frac{n\omega}{c} = (n^* + ik)\frac{\omega}{c} \quad (2.12)$$

On substituting equation (2.12) into equation (2.10) we obtain

$$E(z,t) = E_0 e^{i(\omega n^* z/c - \omega t)} \quad (2.13)$$

$$E(z,t) = E_0 e^{-(k\omega z/c)} e^{i(\omega n z/c - \omega t)} \quad (2.14)$$

This shows that a non-zero extinction coefficient leads to an exponential decay of the wave in the medium. At the same time, the real part of n still determines the phase velocity of the wave front, as in the standard definition of the refractive index given before in equation (2.2).

The optical intensity of a electromagnetic light I wave is proportional to the square of the electric field, namely $I \propto EE^*$. Therefore deduce from equation (2.14) that the intensity falls off exponentially in the medium

with a decay constant equal to $2\left(\frac{k\omega}{c}\right)$. On comparing this to Beer's law given in equation (2.4) we conclude that

$$\alpha = \frac{2k\omega}{c} = \frac{4\pi k}{\lambda} \quad (2.15)$$

where λ is the free space wavelength of light. This shows us that k is directly proportional to the absorption coefficient [20].

The knowledge of real and imaginary parts of complex refractive index, as a function of wavelength (frequency), is necessary to make effective use of these materials for optoelectronic devices [42].

The variation of refractive index with doping and growth parameters also provides the means to tailor the refractive index to any desired value required for use in filters [43].

The refractive index of an optical or dielectric medium, n , was given in equation (2.2).

Using equation (2.2) and Maxwell's equations, one obtains the well known Maxwell's formula for the refractive index of a substance as

$$n = \sqrt{\epsilon_r \mu_r} \quad (2.16.a)$$

where ϵ_r is the static dielectric constant and μ_r is the relative permeability.

As $\mu = 1$ for non magnetic substances, one gets

$$n = \sqrt{\epsilon_r} \quad (2.16.b)$$

which is very useful in relating the dielectric properties to optical properties of materials at any particular frequency of interest. As ϵ_r depends on the wavelength of light, the refractive index also depends on the wavelength of light, and this dependence is called dispersion. In

addition to dispersion, an electromagnetic wave propagating through a lossy medium experiences attenuation, which means it loses its energy, due to various loss mechanisms such as the generation of phonons (lattice waves), photogeneration, free carrier absorption, scattering, etc. in such materials, the refractive index becomes a complex function of the frequency of the light wave. The complex refractive index, denoted usually by \mathbf{n}^* , is related to the complex relative dielectric constant, $\epsilon_r = \epsilon'_1 + i\epsilon''_2$ by

$$\mathbf{n}^* = \mathbf{n} + i\mathbf{k} = \sqrt{\epsilon_r} = \sqrt{\epsilon'_1 + i\epsilon''_2} \quad (2.17)$$

The real part of \mathbf{n}^* , namely \mathbf{n} , is the same as the normal refractive index defined in ($\mathbf{n} = c/v$), \mathbf{k} , is the extinction coefficient. And ϵ'_1 and ϵ''_2 are respectively, the real and imaginary parts of ϵ_r .

Equation (2.17) gives

$$\epsilon'_1 = \mathbf{n}^2 - \mathbf{k}^2 \quad \text{and} \quad \epsilon''_2 = 2\mathbf{n}\mathbf{k} \quad (2.18)$$

In explicit terms, \mathbf{n} and \mathbf{k} can be obtained as

$$\mathbf{n} = (1 / 2^{1/2}) [(\epsilon'^2_1 + \epsilon''^2_2)^{1/2} + \epsilon'_1]^{1/2} \quad (2.19.a)$$

$$\mathbf{k} = (1 / 2^{1/2}) [(\epsilon'^2_1 + \epsilon''^2_2)^{1/2} - \epsilon'_1]^{1/2} \quad (2.19.b)$$

This analysis shows us that \mathbf{n}^* and ϵ_r are not independent variables, if we know ϵ'_1 and ϵ''_2 we can calculate \mathbf{n} and \mathbf{k} , and vice versa.

These equations show us that the refractive index is basically determined by the real part of the dielectric constant, while the absorption is mainly determined by the imaginary part. This generalization is obviously not valid if the medium has a very large absorption coefficient.

The optical constants n and k can be determined by measuring the reflectance from surface of a material. For normal incidence from air, the reflection coefficient, r , is obtained as

$$r = \frac{1-n^*}{1+n^*} = \frac{1-n+jk}{1+n-jk} \quad (2.20)$$

The reflectivity R is then defined by

$$R = |r|^2 = \left| \frac{1-n+jk}{1+n-jk} \right|^2 = \frac{(1-n)^2+k^2}{(1+n)^2+k^2} \quad (2.21)$$

Solving equation (2.21) for n gives:

$$n = \left\{ \frac{(1+R)}{(1-R)} \right\} \pm \left\{ \left[\frac{(1+R)}{(1-R)} \right]^2 - (1+k^2) \right\}^{1/2} \quad (2.22)$$

This equation gives the coefficient of reflection between the medium and the air (or vacuum) at normal incident [31].

In a transparent material such as glass in the visible region of spectrum, the absorption coefficient is very small. Equations (2.17) and (2.19.b) then tell us that k and ϵ_r may be taken as real numbers. This is why tables of properties of optical materials generally list only the real parts of the refractive index and dielectric constant. Whenever k is large, for example over a range of wavelengths, the absorption is strong, and the reflectance is almost unity. The light is reflected, and any light in the medium is highly attenuated [31].

2.6. Dispersion of the refractive index within the Wemple-DiDomenico (WDD) single-oscillator dispersion model

Among the most important parameters characterizing the optical materials as optical fibers can be determined from the energy dispersion

of refractive index. The knowledge of accurate values of the wavelength dependent complex refractive index of thin solid films is very important, both from a fundamental and technological viewpoint, the dispersion behavior, as we all known, plays an important role in the research for optical materials, because it is a significant factor in optical communication and in designing devices for spectral dispersion. The spectral dependence data of the refractive index were evaluated according to the single-

effective-oscillator model proposed by Wemple and DiDomenico [15] and Wemple [16]. Those authors searched dispersion data for more than one hundred different covalent, ionic, crystalline and amorphous materials. They found that all the optical data could be described, to a very good approximation, by the following formula

$$n^2(E) - 1 = \frac{E_d E_0}{E_0^2 - (hv)^2} \quad (2.23)$$

where $n(E)$ is the refractive index at photon energy $hv \rightarrow 0$, ν is the frequency, h is Planck constant, E_d is the electronic dispersion energy. The dispersion energy [30] is a measure of the average strength of interband optical transitions, E_0 is the single oscillator energy [44].

The oscillator energy is an "average" energy gap (Wemple –DiDomenico "gap") and inclose approximation, it scales with the Tauc gap, E_g^{opt} , $E_0 \approx 2E_g^{opt}$. While the parameter E_d , which is a measure of the intensity of the inter-band optical transition, does not depend significantly on the band gap [45].

2.7. Relation between optical energy gap and chemical composition

It was found that there is a number of correlations between the chalcogenide glass forming ability and some parameters such as the average coordination number $\langle r \rangle$ and average heat of atomization H_s . An attempt has been made to evaluate this correlation according to simple criterion for computing the ability of a chalcogenide system to retain its vitreous states. Therefore it was necessary to present these parameters.

2.7.1. The average heat of atomization

The heats of atomization of the elements provide a direct measure of cohesive energy and consequently of the relative bond strengths. The heat of atomization in kCal/mole of atoms, is the quantity of heat energy required to change one mole of an element in its standard state at 298 K to gaseous atoms.

For a binary semiconductor formed from atoms A and B, according to Pauling [46], the heat of atomization H_s (A-B), is the sum of the formation heats ΔH and the average heats of atomization H_s (A-B). In other words, it corresponds to the average non-polar bond energy of two atoms which given by

$$H_s(A - B) = \Delta H + \frac{1}{2}(H_s^A + H_s^B) \quad (2.24.a)$$

The first term in equation (2.24.a) is proportional to the square of the difference between the electro- negativity X_A and X_B of the two atoms

$$\Delta H \propto (X_A - X_B)^2 \quad (2.24.b)$$

In the few materials for which known, the amount of heat of formation ΔH is about 10% of the heat of atomization and is therefore neglected. Hence H_s is given quite well by

$$H_s(A - B) = \frac{1}{2}(H_s^A + H_s^B) \quad (2.25)$$

In order to extend this idea to ternary and higher order semiconductor compounds, the average heat of atomization of H_s is defined for a compound $A_\alpha B_\beta C_\gamma$ as a direct measure of the average bond strength as

$$H_s = \frac{(\alpha H_s^A + \beta H_s^B + \gamma H_s^C)}{(\alpha + \beta + \gamma)} \quad (2.26)$$

Where α , β and γ are the ratios of Ge, Te and Cu in the alloy.

2.7.2. The average coordination number

The simple physical requirement that the number of constraints in an amorphous material equals the number of degrees of freedom in the space that material occupies (or network dimensionality) defines a relatively simple criterion for an ideal, strain-free thin film or bulk material [47]. For an ideal glass in three dimensions, the bond constraint metric is 3, so that the average number of bonds/ atoms, C_{av} is given by

$$C_{av} = 3 \quad (2.27)$$

This simple criterion provides the basis for the application of Bond of Constraint Theory (BCT) for discriminating between materials with

different degrees of ideality in the context of the ease of glass formation. When it is met, $C_{av} = 3 \pm 0.1$, a material may be considered to be a "good glass-former". This criterion will be important in identifying the ease of reversible optical or electrical switching in thin film amorphous materials

for memory applications. We start with the basic assumption [48] that for an "ideal" glass, the average number of constraints is 3. Then we expand the number of constraints in terms of the stretching and bending constraints. Defining $\langle r \rangle$ as the average coordination, we get an important relation between the number of constraints and the average coordination

$$C_{av} = (5/2) \langle r \rangle - 3 \quad (2.28)$$

So now the "ideal glass" [49] has an average coordination number

$$\langle r \rangle = 2.40 \quad (2.29)$$

This is equivalent to an average number of constraints per atom of 3.

Loffe and Regwl [50] have suggested that the bonding character in the nearest-neighbor region, which means the average coordination number $\langle r \rangle$, characterizes the electronic properties of semiconducting materials. The average coordination number $\langle r \rangle$ in ternary compounds $Ge_xTe_yCu_z$ ($x + y + z = 1$), is generalized as [49]

$$\langle r \rangle = (xCN(Ge) + yCN(Te) + zCN(Cu)) \quad (2.30)$$

where x, y and z is concentration of the Ge, Te and Cu respectively and $CN(Ge)$, $CN(Te)$ and $CN(Cu)$ is the coordination number of Ge, Te and Cu respectively.

The glass-forming ability of Ge-Te glasses doped with Cu can be understood on the basis of the Phillips constraint theory proposed for covalent network glass [48].

The constraint theory suggests that covalent network glasses (chalcogenide glasses) consists of under-cross-linked floppy and over-constrained rigid networks. It also predicts a critical composition corresponding to an average coordination number $\langle r \rangle = 2.40$, at which the number of constraints (bond-stretching and bond-bending forces) acting on the network are balanced by the number of freedom available for the atoms in network. So glasses with $\langle r \rangle$ less than 2.40 are under-cross-linked or loosely connected, and glasses with $\langle r \rangle$ greater than 2.40 are over constrained or rigidly connected. A transformation from a floppy to a rigid network structure called rigidity percolation threshold occurs at $\langle r \rangle = 2.40$. Glass-forming ability of many alloys is generally found to be easy at the composition (corresponding to $\langle r \rangle = 2.40$) at which the rigidity percolation threshold occurs [50].

In addition to the rigidity percolation threshold, a chemical ordering also occurs in chalcogenide glasses (usually at higher coordination number), where the structural network is maximally ordered. Maximum ordering in the network indicates that they are closest to its crystalline state. The glass-forming ability of chalcogenide glasses is found to be difficult at the composition corresponding to the chemically ordered network as they attain their crystalline state easily. Unusual changes in various properties are expected at these critical compositions [50].

2.8. Literature Survey

2.8.1. Structure Study

Amorphous Ge and other amorphous semiconductors of tetrahedrally bonded (coordinated) elements, exhibit electronic and structural flexibility, which facilitate removal the dangling bonds. As consequence, a typical chalcogenide, has a relatively sharp absorption edge. The amorphous chalcogenide exhibit an exponential absorption tail (Urbach tail) followed by a behavior, $(\alpha h\nu)$ proportional to $(h\nu - E_g^{opt})^r$ at higher photon energies (above the Urbach tail). The shift in the absorption edge towards longer wavelength (increased absorption) suggest the creation of additional gap states near the band edges.

The Ge-Te system is very attractive since it allows the formation of glasses in the range of $x = 0.0$ to about $x = 0.42$ at.%. Furthermore the variation of x induces significant changes in the optical properties related to electronic structure. Electronic transition in many amorphous semiconductors give rise to an the optical absorption edge.

V.M. Goldschmidt [52] introduced the idea of thinking of the glass structure in terms of their atomic arrangements, the relative size and valances of the atoms or ions concerned.

I.S. Dutsyak [53] studied the short range order structure and physical properties of amorphous Ge-Te thin films. Their short range order was described by the model of a tetrahedral environment of atoms with coordination 4(Ge) and 2(Te). Films of amorphous Ge-Te are semiconductors of lone pair type, the majority carriers are holes, he found

that the width of optical gap is 0.7-0.8 eV, and the thermal activation energy of conduction is 0.3-0.4 eV.

2.8.2. Optical and physical properties of amorphous thin films

A.H. Ammar [54] prepared five $Zn_xCd_{1-x}Te$ thin films with $x = 0.1, 0.3, 0.5, 0.7$ and 0.9 at %, their optical constants were determined.

He found that, the refractive index n and extinction coefficient k decreased as x increases from 0.1 to 0.9, and the spectral dependence of the absorption coefficient α indicated direct allowed transitions for all tested film compositions.

A.S. Abd-Rabo et al. [39], studied the optical properties of $Bi_{30}Se_{70-x}Te_x$ amorphous thin films (where $x = 35, 40$ and 45 at %) and found that the optical absorption was due to indirect transitions and the energy gap decreased with increasing Te content, the decrease in the energy gap may be explained by Kastner [55]. The value of the index of refraction n was found to be higher than the extinction k through the investigated range.

Afaf et al. [56] studied the optical properties of $As_{25}Ge_{45}Se_{30}$, $As_{25}Ge_{35}Se_{40}$ and $As_{25}Ge_{40}Se_{35}$ thin films. The results indicated E_g^{opt} decreased with increasing Se content and the type of transition in the non-crystalline material was found to be indirect transition.

H.E Atiya et al. [57] studied the optical properties of $Se_{85}Te_{10}Bi_5$ thin films, they found that comparing the obtained values of E_g^{opt} (1.32 eV) with that of obtained before in a past study [4] for $Se_{85}Te_{15}$ thin films

(1.09 eV), it was found that the addition of Bi to the $\text{Se}_{80}\text{Te}_{20}$ increased the E_g^{opt} .

M.M. Abdel-Aziz et al. [58] studied the optical properties of $\text{Ge}_1\text{Se}_{9-x}\text{Te}_x$ thin film of different of various thicknesses range of (114-618.3 nm) as a function of Thallium contents. They found that the coefficient n increases with the increase in the Thallium contents. This may be due to the increase in density (N) and hence, to the decrease in the optical band gap E_g^{opt} .

E.A. Mahmoud et al. [37] studied optical absorption of $\text{Ge}_x\text{Fe}_x\text{Se}_{100-2x}$ ($0 \leq x \leq 15$) amorphous thin films as a function of composition and thickness. The optical absorption measurements indicated that the absorption mechanism was due to indirect transitions and E_g^{opt} increased while E_t decreased with increasing both Ge and Fe content.

The dependence of band tail on the absorption spectra of amorphous materials was usually related to the distribution of localized states in the valance band tail. It was sensitive to the structure and disorder level in amorphous materials and could provide information on the changes in material network induced by various $\text{Ge}_x\text{Fe}_x\text{Se}_{100-2x}$ reasons [59].

Pankaj Sharma et al. [60] calculated the optical constants of $\text{Ge}_{10}\text{Se}_{90-x}\text{Te}_x$ ($x = 10,20,30,40$ and 50) thin films using the Swanepoel method. It was found that the optical band gap is indirect in nature and decreases with the increase of Te content in $\text{Ge}_{10}\text{Se}_{90-x}\text{Te}_x$ thin films. They suggested that the

decrease of the optical gap with Te content can be correlated with the character of the chemical order of chalcogenide amorphous semiconductors. It was found that the addition of Te in the glass structure

causes deeper band tails extended in the gap and thereby leading to a decrease in the value of optical band gap.

2.8.3. Composition dependence of the optical properties of amorphous thin films

E.R Shaaban [61] studied the composition dependence of the optical properties of $\text{Ge}_{10}\text{As}_x\text{Se}_{90-x}$ thin films, the straightforward analysis proposed by Swanepoel was successfully employed. The results indicated that the values of n gradually increase with increasing As content. The results indicated that the value of E_g^{opt} decreased with increasing the amount of As at the expense of Se.

M. Dongol, et al. [62] studied the composition effect on the structural and optical properties of $\text{Ge}_{15}\text{Te}_{85-x}\text{Cu}_x$ ($0 \leq x \leq 7$) thin films. The optical energy gap E_g^{opt} of the deposited films was determined from the absorption and transmission spectra. They found that the absorption in $\text{Ge}_{15}\text{Te}_{85-x}\text{Cu}_x$ thin films is due to in-direct transition. The indirect optical energy gap decreased slightly as the Cu content increased. It was noticed that ϵ_∞ and N/m^* , and n increase with increasing Cu content.

A.B. Abd-El-Moiz et al. [63] presented a new study for the composition dependence of optical properties of $\text{As}_{20}\text{Se}_{80-x}\text{Tl}_x$ thin films.

They found that the absorption in As–Se–Tl was due to non-direct transition, he also found that the optical band gap, E_g^{opt} decreased with the increase of Tl concentration. The dispersion of refractive index in As–Se–Tl was analyzed using the concept of the single oscillator and was expressed by the Wemple–DiDomenico relationship, the dependences of

the optical gap E_g^{opt} and the single oscillator energy E_0 on composition were found that, E_0 , decreases with slow rate as Tl-content increases up to $x = 20$ at% and then the high decreasing rate is introduced.

D.D. Strbac et al. [64] discussed the dispersion of the refractive index in terms of the single oscillator model proposed by Wemple and DiDomenico for $Cu_x[As_2(S_{0.5}Se_{0.5})_3]_{100-x}$ thin films. Values of E_0 were found to be from 3.92 to 4.03 eV and E_d was found to be 19.92 to 21.7 eV depending on the particular sample. Refractive index values were found to be in the range 2.438-2.530.

J.M. Gonzalez-Leal et al. [65] studied $As_{20}Se_{80-x}Tl_x$ thin films optical properties. They found that the decreasing of the single oscillator energy E_0 with increasing Tl content could be attributed to the dissolving of Tl atoms with bigger atomic radius than Se atoms forming Se–Tl bonds with the longest bonding distances, hence, decrease Se–Se bonds.

N. El-Kabany studied [66] the dependence of Ge_xTe_{1-x} ($0.125 \leq x \leq 0.225$) amorphous thin films as a function of composition. It was found that the allowed direct transitions are responsible for the absorption of Ge-Te films of all compositions. The observed behavior optical properties was explained on the theoretical, Band Constraint Theory (BCT). The results of the work indicated that, the physical properties of the Ge_xTe_{1-x} thin films did not change monotonically with x . The optical gap increased with increasing the Ge content for ($x > 0.20$), this indicated that there are two transitions that existed in the studied glasses. In particular ($x < 0.20$) films were flexible, while the onset of local rigidity occurring at ($x = 0.20$), while at ($x > 0.20$) they became stressed-rigid.

N. El-Kabany et al. [67] studied the composition dependence of $\text{In}_x\text{Se}_{1-x}$ ($0.05 \leq x \leq 0.30$) thin films. The optical band gap was appropriately fitted to the non-direct transition model proposed by Tauc. The results indicated that the value of E_g^{opt} decreased with the increase in the amount of In content and both n and k at any wavelength increased with increasing In content. The subsequent fitting of the refractive index to the single oscillator model (the Wemple-DiDomenico relationship). The single oscillator energy E_0 decreased with increase In content and both dispersion energy E_d and refractive index $n(0)$ were found to increase.

A.A. Al-Ghamdi [34] studied the optical constants for $\text{Se}_{96-x}\text{Te}_4\text{Ag}_x$ amorphous thin films. He found that the optical absorption measurements on the deposited amorphous $\text{Se}_{96-x}\text{Te}_4\text{Ag}_x$ films indicated that the absorption mechanism was due to indirect transition and that the optical gap increased with increasing Ag content ,the increase in optical band gap may be due to the decrease in the amount of disorder in the materials and decrease in the density of defect states (which results in the reduction of tailing of bands).

M. Krbal et al. [68] analyzed the dispersion data of the $\text{Ag}_x(\text{As}_{0.33}\text{S}_{0.67-y}\text{Se}_y)_{100-x}$ thin films on the basis of the Wemple-DiDomenico single-oscillator model, oscillator strength E_d increased with increasing Ag. The E_d value was related to the bond length. Index of refraction increased with increasing Ag and Se content.

2.8.4. Effect of addition of metals on optical properties of amorphous thin films

The doping of chalcogenide glassy semiconductors with metal (copper) is an effective way of changing the electrical and other properties of glasses in a definite direction. This problem has been extensively studied for many years [69].

In recent studies, the addition of copper to amorphous $\text{Ge}_{15}\text{Te}_{85}$ films was found to result in some interesting features. The diminution of disorder and defect in the structural bonding is known to increase the optical energy gap.

A.E. Bekheet et al. [70] studied the effect of Ag addition on the optical properties of $\text{Se}_{90}\text{Te}_{10}$ ($0 \leq x \leq 6$) films. They found that the values of n and k decreases with increasing the wavelength through the investigated range, as well as, its decrease with Ag addition. Value of the E_g^{opt} increased by increasing Ag content, this increase may be due to the increase in grain size, the reduction in the disorder and the decrease in density of defect states (which results in the reduction of tailing of bands)

S.A. Fayek et al. [71] studied the effect of copper addition on optical and electrical properties of $\text{As}_{10}\text{Se}_{90}$ ($0 \leq x \leq 1$ at.%) thin films. They reported that the analysis of the obtained data showed that the involved transition mechanisms was allowed indirect since line dependence is obtained at $r = 2$. The E_g^{opt} was in the range 1.47-1.53 eV, and it decreased with increasing the Cu content.

2.8.5. Effect of composition on the heat of atomization

Chalcogenide liquids of the average coordination number $\langle r \rangle = 2.40$ undergo the least number of configurational rearrangements in transforming to a glass, hence, such compositions were found to be the best glass-formers as A.K. Varshneya, reported [9]. He studied physical properties of chalcogenide glasses as a function of the average coordination number.

The values of H_s for $\text{Ge}_x\text{Se}_y\text{Ag}_{100-x-y}$ alloys (with $x = 15$ and $y = 85, 75$ and 65) were found to be increasing with the addition of Ag as reported by A.H. Ammar et al [54]. They also found that the E_g^{opt} is correlated with H_s .

N. El-Kabany [66] found that the average coordination number for $\text{Ge}_x\text{Te}_{1-x}$ ($0.125 \leq x \leq 0.225$) amorphous thin films increases with increase of Ge content which gives an indication that the number of constraints increases hence the value of optical gap will strongly depend on heat of atomization.

N. El-Kabany et al. [67] discussed the relationship between optical gap and chemical composition in $\text{In}_x\text{Se}_{1-x}$ ($0.05 \leq x \leq 0.30$) thin films in terms of the average heat of atomization H_s and average coordination number. They found that additional of In in the system leads to increase $\langle r \rangle$ and H_s .

L.A. Wahab et al. [72] related the optical gap with the chemical bond energy, and calculated the values of heat of atomization of $\text{Ge}_{1-x}\text{Se}_2\text{Pb}_x$

($x = 0, 0.2, 0.4, 0.6$) thin films. They found that H_s decreased with increasing the Pb content, i.e. the average bond of the compound .

3.1. Introduction

This chapter contains the description of the preparation of $\text{Ge}_{15}\text{Te}_{85-x}\text{Cu}_x$ glasses as ingots and also the preparation of $\text{Ge}_{15}\text{Te}_{85-x}\text{Cu}_x$ thin films. The film specimen design is described. The structure examination for bulk and films, which include X-ray diffraction are also described in details. Finally the method of optical absorption measurements was described.

3.2. Material preparation

3.2.1. Preparation of bulk material $\text{Ge}_{15}\text{Te}_{85-x}\text{Cu}_x$

$\text{Ge}_{15}\text{Te}_{85-x}\text{Cu}_x$ ($2 \leq x \leq 6$, at. %) chalcogenide glasses were prepared using high purity (99.999 %) Ge, Te and Cu supplied by from Aldrich Chemical Company Co, UK. The proper amount for each material was then weighted in accordance with their atomic percentage into a quartz tube. The tubes were of 0.9 cm internal diameter, 0.1 cm thick and 20 cm in length. To avoid the oxidation of the sample, the contents of the ampoule for each composition were sealed under vacuum of 10^{-4} Torr. Since the melting point for each element differs from the other, the ampoules were heated in Heraus programmable tube furnace type RO 7/50 operated at 1373 K. During the melt process for 25 hours, the ampoules were frequently agitated in order to intermix the constituents to ensure a high degree of homogeneity of the

melt. The melt was rapidly quenched into ice-cold water at 0°C resulting in a bulk glass of the required chemical composition, $\text{Ge}_{15}\text{Te}_{85-x}\text{Cu}_x$ ($2 \leq x \leq 6, \text{at. \%}$). Quenched samples were removed from the ampoules by breaking the quartz ampoules. The quenched glass was then finely ground. The compositions of the prepared glasses are given in table (3.1)

Table (3.1) Composition of the prepared $\text{Ge}_{15}\text{Te}_{85-x}\text{Cu}_x$ amorphous samples

Sample Number	Composition at .%		
	Ge_{15}	Te_{85-x}	Cu_x
1	15	83	2
2	15	82	3
3	15	81	4
4	15	80	5
5	15	79	6

3.2.2. Preparation of $\text{Ge}_{15}\text{Te}_{85-x}\text{Cu}_x$ thin films

Different methods of preparation of semiconducting films include :

- i: Direct thermal evaporation (which was used in preparing the samples for the present study),**
- ii: Flash evaporation,**
- iii: Electron beam evaporation,**
- iv: Sputtering**

The structure and properties of the films are very sensitive to their preparation procedure. To reduce the relative importance of gaseous contamination of interdiffusion and to achieve rapid fabrication of actives, it is desirable to deposit films at higher rates.

Direct thermal evaporation

Amorphous Ge-Te-Cu films are obtained by standard vacuum thermal evaporation of Ge-Te-Cu bulk glasses. In this method, evaporation was performed from small quartz crucible which was heated with a conical basket of tungsten wire as a filament. The film samples were deposited by thermal evaporation technique onto thoroughly cleaned glass substrates. The evaporation was done under vacuum of 10^{-6} Torr, using Edward Coating Unit Ed-306A. The coating unit is provided with water cooled vapor, diffusion pump E04, with pumping speed of 600 L/Sec. Liquid nitrogen trap was located between the diffusion pump and the high vacuum valve. This trap migrating diffusion pump vapors. The pumping system is also provided a trap which eliminates the back-streaming of oil vapors from the rotary pump.

Evaporation is started by passing a low current for a sufficient period of time in the filament to heat up the material. The current is gradually and carefully increased, when the material melts inside the boat the current passing through the filament is increased fairly quickly. This was done to avoid alloy decomposition. The thickness of films was determined by a thickness monitor. All prepared samples have the same thickness of 200

3.3. Structure examination

3.3.1. X-Ray diffraction

The quenched glass was then finely ground and screened to a particle size of 200 μm powder. The investigation was undertaken to identify crystallized phases, which might be present in the as-prepared glasses.

X-ray diffraction investigation for $\text{Ge}_{15}\text{Te}_{85-x}\text{Cu}_x$ ($2 \leq x \leq 6, \text{at. \%}$) films and powders of different compositions using Philips type 1710 chart diffractometer.

The radiation source was CuK_α and used a graphite monochromator with $\lambda=1.54178 \text{ \AA}$ at 40 kV and 30 mA. The scanning speed was 3.6 deg/min. The scattering angles (2θ) measured between 4 and 110 degrees. All the diffractograms were carried out at room temperature.

3.4. Optical absorption measurements

The absorption $A(\lambda)$ and transmission $T(\lambda)$ at normal incidence for thermally evaporated $\text{Ge}_{15}\text{Te}_{85-x}\text{Cu}_x$ ($2 \leq x \leq 6, \text{at. \%}$) thin films onto non-absorbing substrate were obtained utilizing computerized SHIMADZU UV-2100 double beam spectra photometer. The measurements were carried out in wavelength range 280 to 1000 nm with 5 nm steps. The absorption measurements are carried out against a virgin ultrasonically cleaned substrate which served as a reference. They are done in various parts of the films, scanning the entire sample, and the

obtained spectra are excellently reproduced. All the optical measurements were carried out after samples were slowly cooled at room temperature.

4.1. Introduction

In recent years, thin film science has grown worldwide into a major research area. The importance of thin films explodes through microelectronics, optics and nanotechnology. Chalcogenide glasses are playing a major role in thin film technology due to their optical applications as they are excellent IR transmitting materials. Evaluation of the applicability of an optical material requires knowledge of its optical properties [71].

4.2. Structure information

4.2.1. XRD (X-ray Diffraction)

In the present work, the effect of Cu content on the physical properties of the $\text{Ge}_{15}\text{Te}_{85-x}\text{Cu}_x$ thin films, where ($2 \leq x \leq 6, \text{at.}\%$) was studied.

X-ray diffraction technique was used to check the amorphous nature and homogenization of the ternary Ge-Te-Cu system, the measurements had been carried out using different compositions of $\text{Ge}_{15}\text{Te}_{85-x}\text{Cu}_x$ thin films. The diffraction charts do not show any strong diffraction peaks, and the absence of sharp diffraction lines. The presence of humps only indicating that all the films specimens are amorphous.

The X-ray diffraction charts for $\text{Ge}_{15}\text{Te}_{85-x}\text{Cu}_x$ ($2 \leq x \leq 6$ at. %) thin films are shown in figure (4.1).

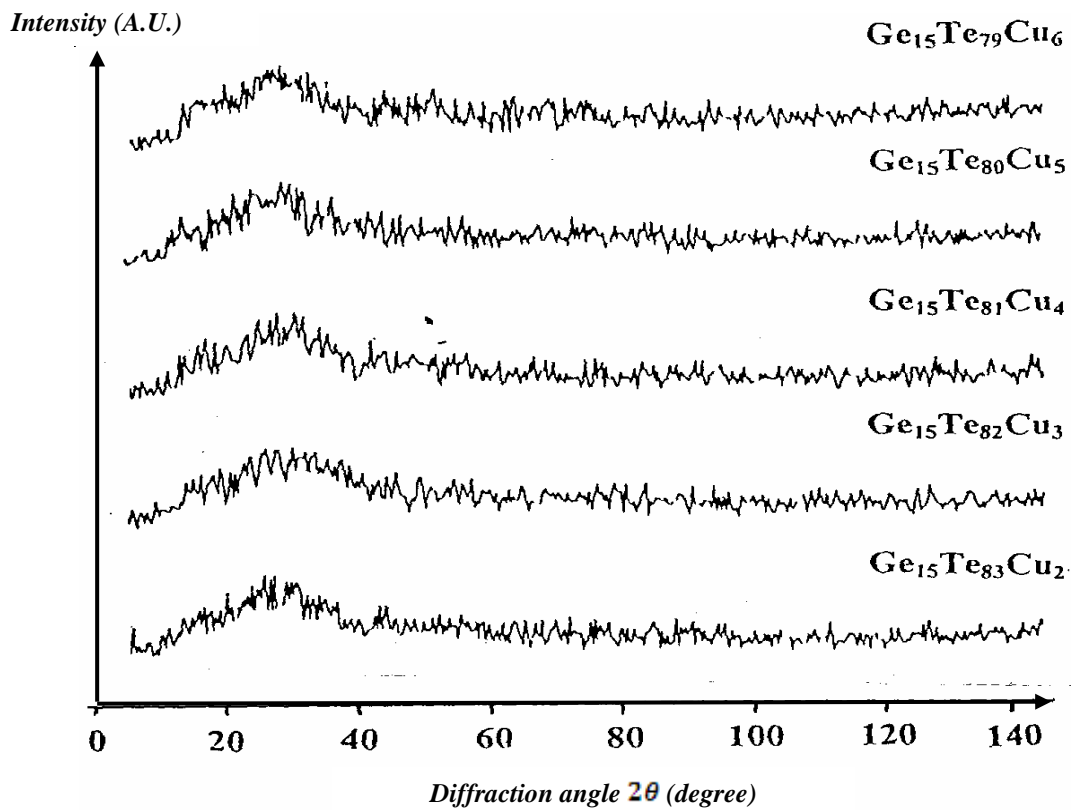


Fig. (4.1) The X-ray diffraction pattern for $\text{Ge}_{15}\text{Te}_{85-x}\text{Cu}_x$ thin films of compositions.

4.3. Determination of optical constants of $\text{Ge}_{15}\text{Te}_{85-x}\text{Cu}_x$ thin films

There are available a number of experimental techniques for measuring n and k . One of the most popular and convenient optical

measurements involves passing light through a thin sample, and measuring the absorption and transmitted intensity as a function of wavelength [$A(\lambda)$ and $T(\lambda)$] using a spectrophotometer. This technique has been applied in this study.

In order to obtain the optical constants for the prepared samples (the refractive index and the extinction coefficient), using experimental values of absorption and transmittance equations mentioned (in Chapter 2) have been applied to conjunction with a designed computer program.

4.3.1. Analysis of absorption coefficient

The values of absorption coefficient for all samples have been calculated using the following equation

$$\alpha = (1/d) \ln (1/A) \quad (2.1)$$

where d is the film thickness, and A is the absorption. Figure (4.2) shows the dependence of the absorption coefficient α on the wavelength λ for samples of different compositions. The determined absorption coefficients are between 2 and $12 \times 10^4 \text{ cm}^{-1}$. It is clear that there is no sharp absorption edge which is a characteristic of glassy state [69]. A shift of the absorption edge (either towards lower or higher energies) could be observed when the semiconductor becomes amorphous. It is seen that the

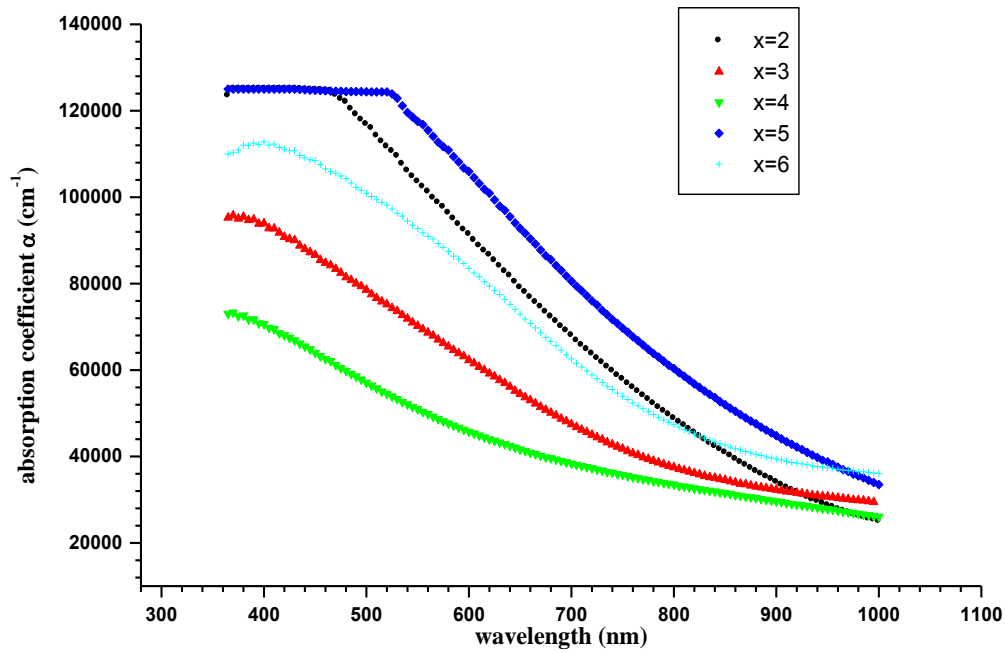


Fig. (4.2) Variation of absorption coefficient α (cm^{-1}) with wavelength λ (nm) for $\text{Ge}_{15}\text{Te}_{85-x}\text{Cu}_x$ thin films of compositions.

position of the fundamental absorption edge shifts to the higher wavelength with increasing Cu content. Figure (4.3) shows a plot between α and $h\nu$ for $\text{Ge}_{15}\text{Te}_{85-x}\text{Cu}_x$ thin films. It is apparent from this plot that the absorption coefficient has an exponential tail, at least down 1.6 eV. It has been observed that the value of α increases linearly with the increase in photon energy for all $\text{Ge}_{15}\text{Te}_{85-x}\text{Cu}_x$ samples.

It can also be seen that there is a shift in the absorption edge towards lower energy with the increase of Cu content.

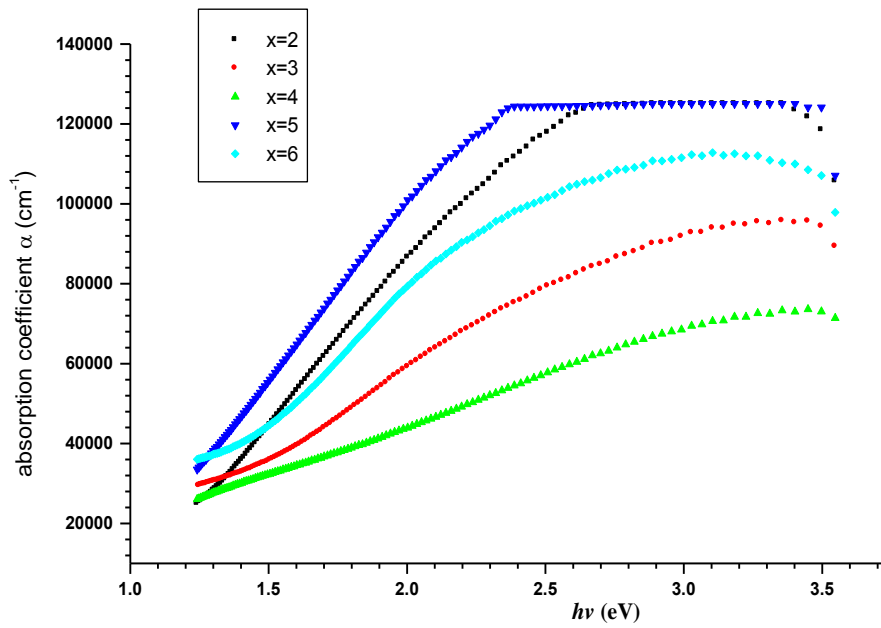


Fig.(4.3) Variation of absorption coefficient α (cm^{-1}) with photon energy $h\nu$ (eV) for $\text{Ge}_{15}\text{Te}_{85-x}\text{Cu}_x$ thin films of compositions.

The effect of composition on optical absorption tails can be observed in both figures (4.2) and (4.3).

4.3.1.1. Determination of extinction coefficient k

The extinction coefficient, k , is easily obtained from the already-known α -values, using equation (2.23). The relation between the extinction coefficient (k) versus photon energy for the $\text{Ge}_{15}\text{Te}_{85-x}\text{Cu}_x$ thin films is shown in figure (4.4). It can be seen that k increases with increasing photon energy. In contrast k decreases with increasing wavelength showing that the fraction of light lost due to scattering and absorbance decreases. All curves exhibit the same trend, a peak is observed in the compound at around 2.25 eV for all five samples. The values of extinction coefficient k increases and shows significant differences followed by decreases with increasing the Cu content in the

alloy for Cu content $x < 4$, then there was an increase in the extinction coefficient for $x \geq 5$.

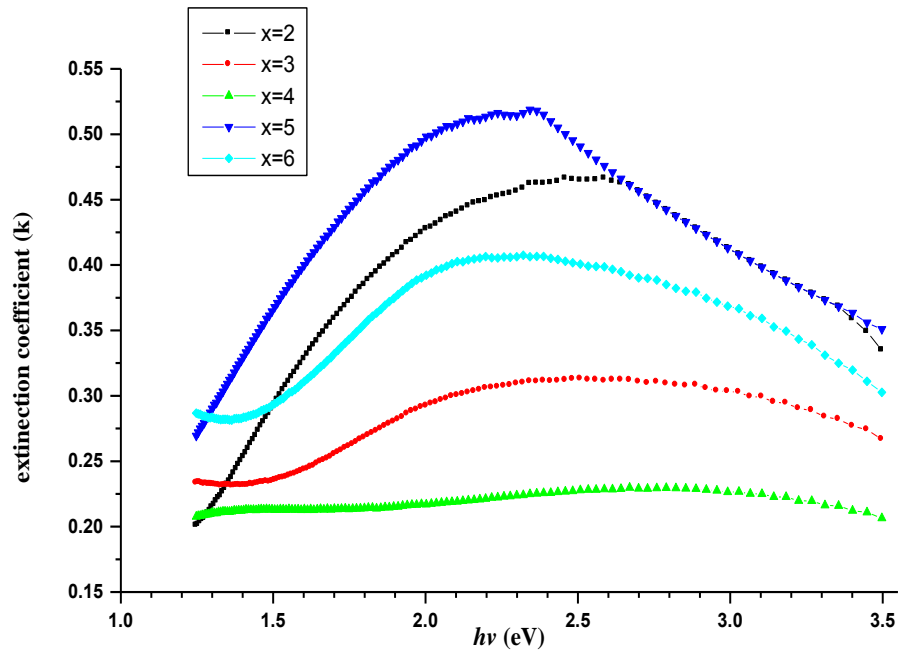


Fig.(4.4) Variation of extinction coefficient (k) with photon energy ($h\nu$) for $\text{Ge}_{15}\text{Se}_{85-x}\text{Cu}_x$ thin films of compositions.

4.3.1.2. Lower values of absorption coefficient (determining Urbach energy)

The incorporation of impurity into the semiconductor often reveals the formation of band tailing in the band gap. At lower values of absorption coefficient $\alpha < 12 \times 10^4 \text{ cm}^{-1}$, the absorption coefficient α depends exponentially on photon energy (Urbach relation). This dependence is known as Urbach rule as given in equation (2.7). Urbach energy (related to the width of the band tail of the localized states at the conduction or valance band edge) generally represents the degree of disorder in an amorphous semiconductor [71].

Figure (4.5) shows the typical variation of $\ln(\alpha)$ versus photon energy ($h\nu$) for all $\text{Ge}_{15}\text{Te}_{85-x}\text{Cu}_x$ thin films.

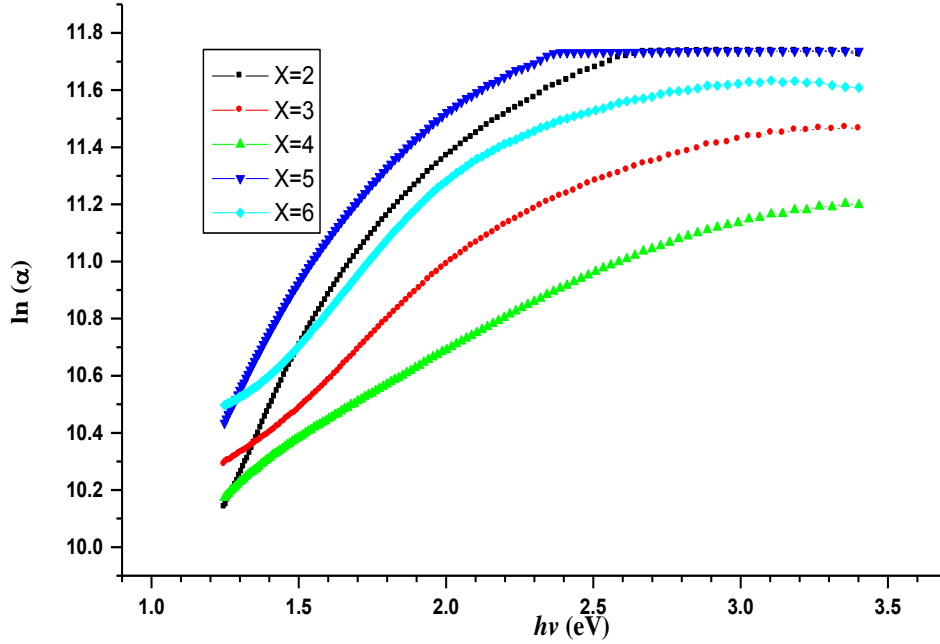


Fig.(4.5) Variation of $\ln(\alpha)$ with $h\nu$ (eV) for $\text{Ge}_{15}\text{Te}_{85-x}\text{Cu}_x$ thin films of compositions.

Using least squares fit, a linear relationship was obtained as shown in figure (4.6).

The inverse of the slope gives the band tail width E_t of the localized states at the band gap. The values of E_t as a function of composition are recorded in table (4.1) which gives the determined values of E_t and β constant as a function of Cu content for $\text{Ge}_{15}\text{Te}_{85-x}\text{Cu}_x$ ($2 \leq x \leq 6$ at. %) thin films. It is observed that the values of E_t varies slightly with increasing the copper content. It is seen that the increase of cohesive energy implies higher bonding strength, i.e. high E_g^{opt} and this means lower defect bonds, which reduces the band tail width [54].

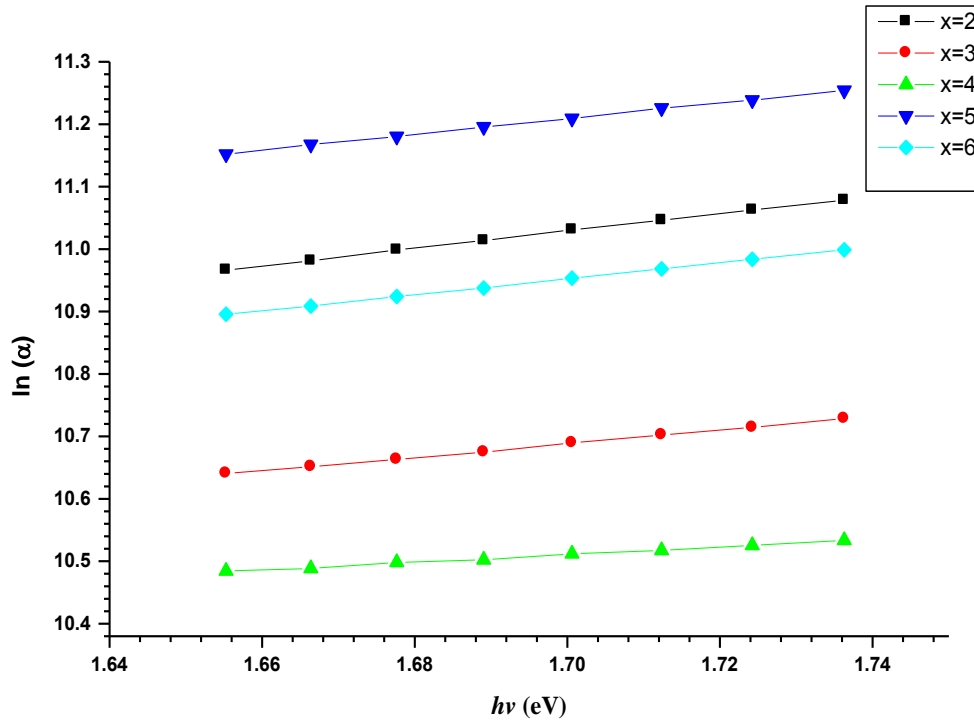


Fig.(4.6) Linear fitting of $\ln(\alpha)$ and photon energy $h\nu$ (eV) for $\text{Ge}_{15}\text{Te}_{85-x}\text{Cu}_x$ thin films of compositions

4.3.1.3. Higher values of absorption coefficient (determination of optical energy gap)

The fundamental absorption edge of the films corresponds to electron transitions from valence band to conduction band and this edge can be used to calculate the optical band gap of the films. The absorption coefficient of amorphous semiconductors, in the high absorption region above the exponential tail, is given according to Tauc [10] by equation (2.5). The relation of $(\alpha h\nu)^{1/r}$ versus $h\nu$ ($r = 1/2, 3/2, 2$ and 3) for all samples of, $\text{Ge}_{15}\text{Te}_{85-x}\text{Cu}_x$ ($2 \leq x \leq 6$ at. %) thin films are shown in figures (4.7) (a, b, c, d and e).

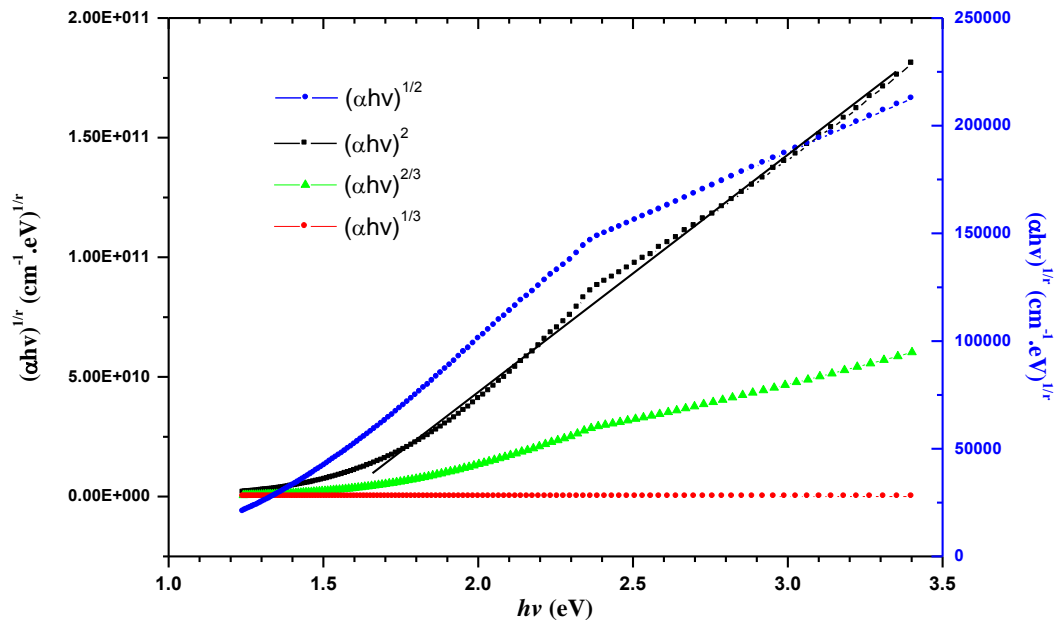


Fig.(4.7.a) The relation between $(\alpha h\nu)^{1/r}$ ($\text{cm}^{-1} \cdot \text{eV}^{1/r}$) versus photon energy $h\nu$ (eV) for $\text{Ge}_{15}\text{Te}_{83}\text{Cu}_2$ thin film.

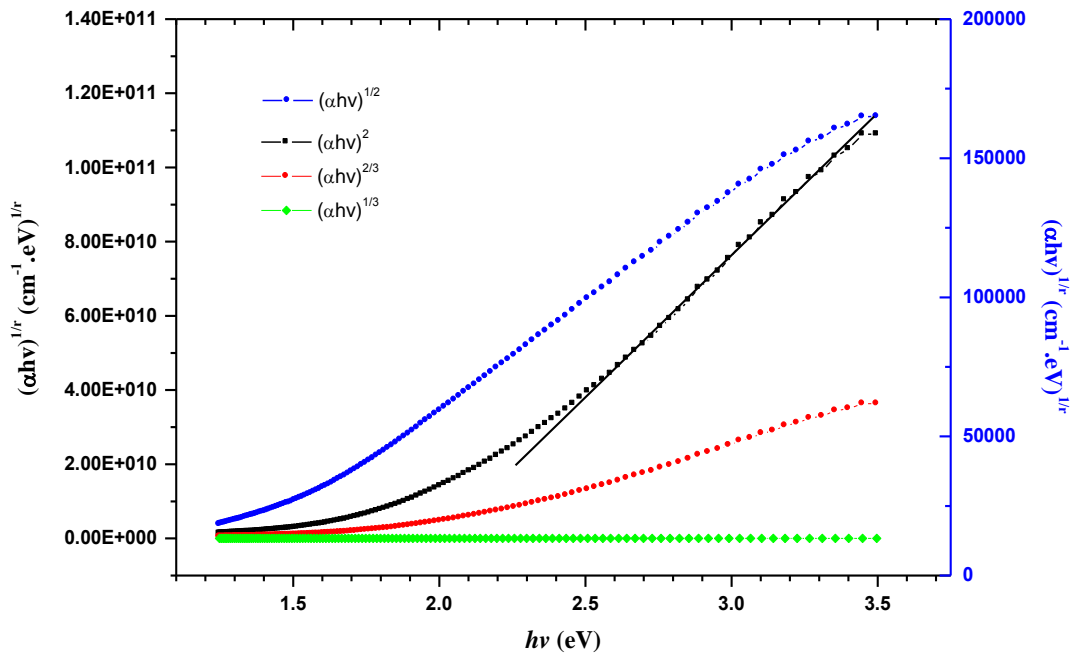


Fig.(4.7.b) The relation between $(\alpha h\nu)^{1/r}$ ($\text{cm}^{-1} \cdot \text{eV}^{1/r}$) versus photon energy $h\nu$ (eV) versus photon energy for $\text{Ge}_{15}\text{Te}_{82}\text{Cu}_3$ thin film.

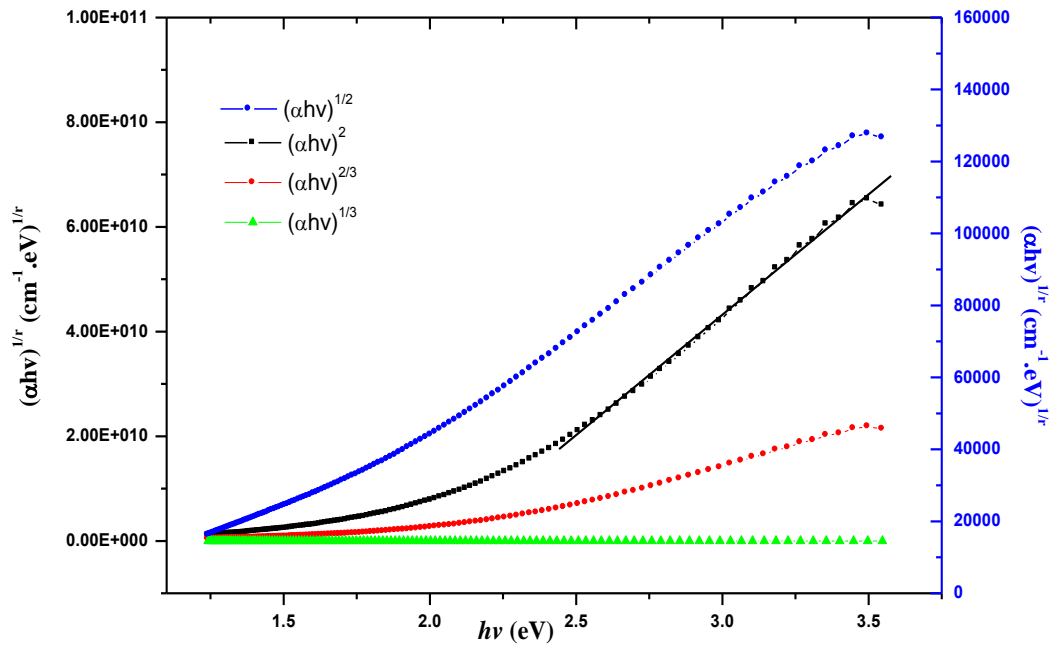


Fig.(4.7.c) The relation between $(\alpha hv)^{1/r} (\text{cm}^{-1} \cdot \text{eV})^{1/r}$ versus photon energy $h\nu$ (eV) versus photon energy for $\text{Ge}_{15}\text{Te}_{81}\text{Cu}_4$ thin film.

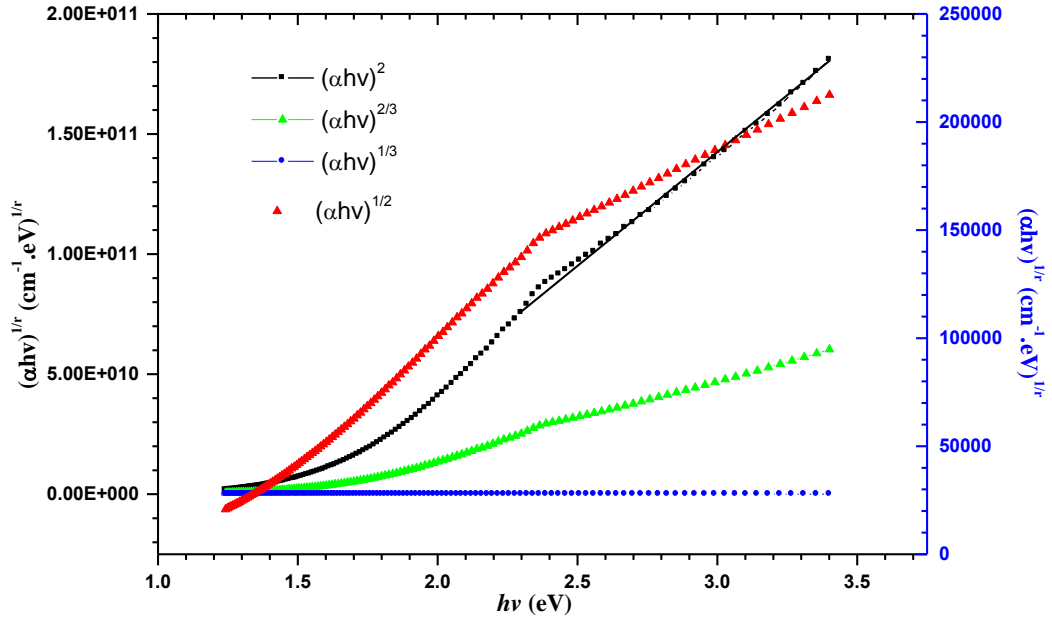


Fig.(4.7.d) The relation between $(\alpha hv)^{1/r} (\text{cm}^{-1} \cdot \text{eV})^{1/r}$ versus photon energy $h\nu$ (eV) versus photon energy for $\text{Ge}_{15}\text{Te}_{80}\text{Cu}_5$ thin film.

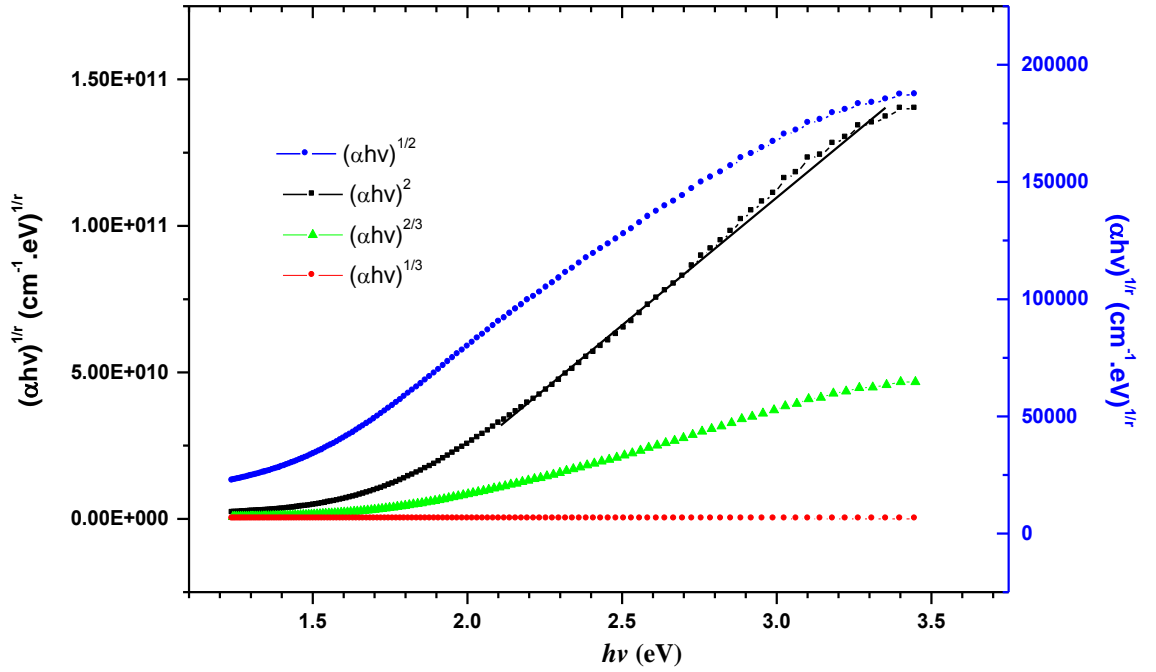


Fig.(4.7.e) The relation between $(\alpha h\nu)^{1/r} (\text{cm}^{-1}.\text{eV})^{1/r}$ versus photon energy $h\nu$ (eV) versus photon energy for $\text{Ge}_{15}\text{Te}_{79}\text{Cu}_6$ thin film.

By plotting graphs of $(\alpha h\nu)^{1/r}$ against $h\nu$ for all possible values of n , it is possible to determine what value of n gives a better fit to the data. Analysis of the obtained data shows that the value $r = 1/2$ shows a linear relation most fit for equation (2.5). This indicates that the involved transition mechanisms are **allowed direct transition** for all our investigated samples.

The values of E_g^{opt} and β can be readily calculated from the plot of $(\alpha h\nu)^2$ versus photon energy ($h\nu$), and can be estimated by the intercept of the extrapolations to zero absorption with the photon energy axis $(\alpha h\nu)^2 = 0$. The constant β was determined from the slope of the linear part of the relation $(\alpha h\nu)^2 = \beta(h\nu - E_g^{\text{opt}})$. Values of the optical energy gap E_g^{opt} and β are given in table (4.1).

The value of E_g^{opt} was estimated using figures (4.8) a, b, c, d and e. In figure (4.9), the shifting in the curve can clearly be shown clearly, as the composition of copper content changes (increases), the same behavior was observed by M. Dongol et al. [71] and C. Harikuttan Unnithan et al. [72]. It can be noticed from the figure that the decrease of E_g^{opt} can be divided into two decreasing rates, the first is slow decreasing from 1.79 eV to 1.69 eV, then there was a slightly decreasing rate at x=4 at.% followed by a high decreasing rate at x=5 at.% ($E_g^{opt} = 1.49$ eV), obtaining a minimum value of E_g^{opt} at x=5 at.%. The decrease of the optical gap with Cu content can be correlated with the character of the chemical order of chalcogenide

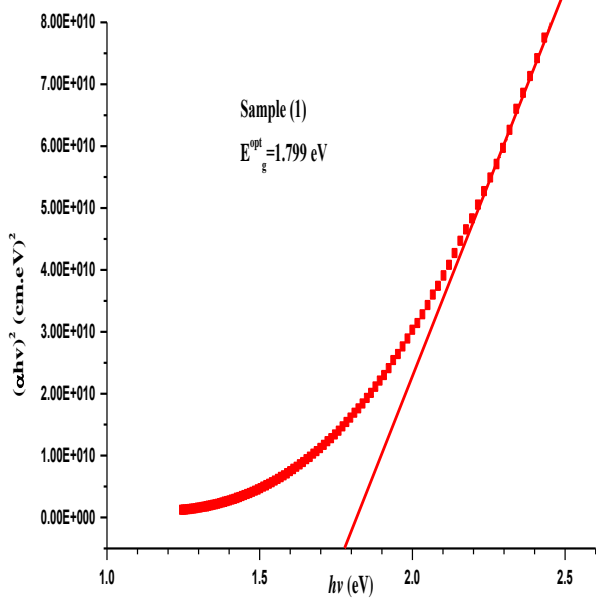


Fig.(4.8.a)

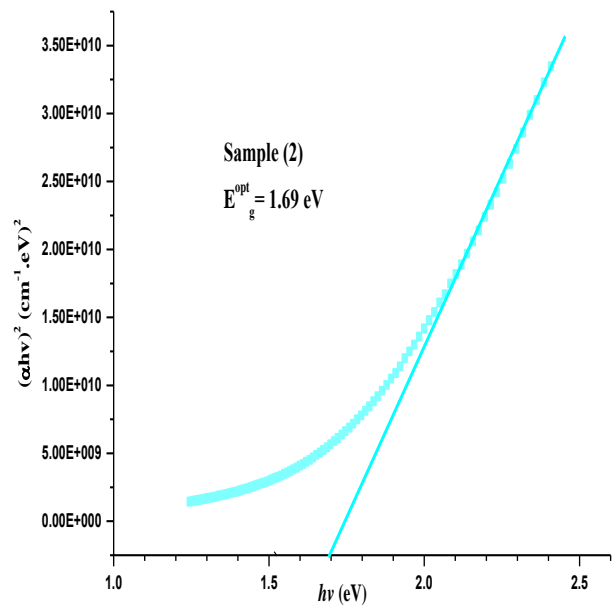


Fig.(4.8.b)

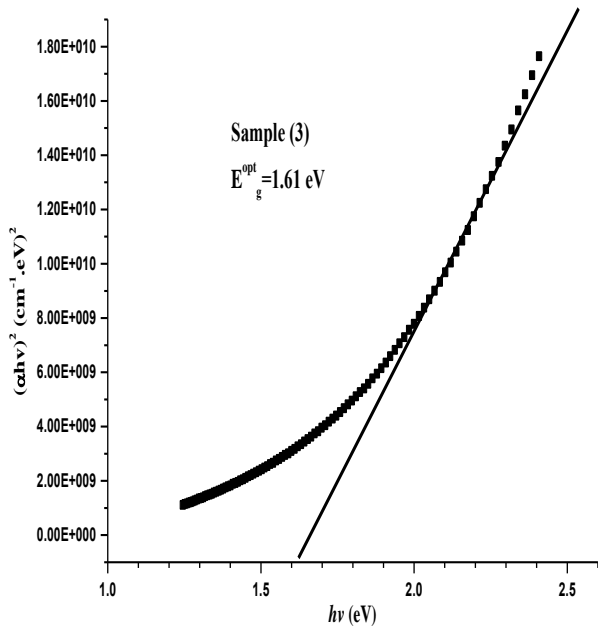


Fig.(4.8.c)

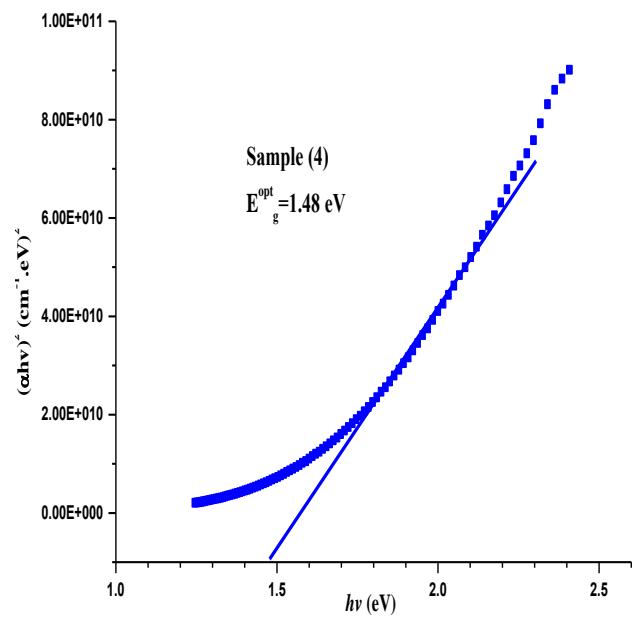


Fig.(4.8.d)

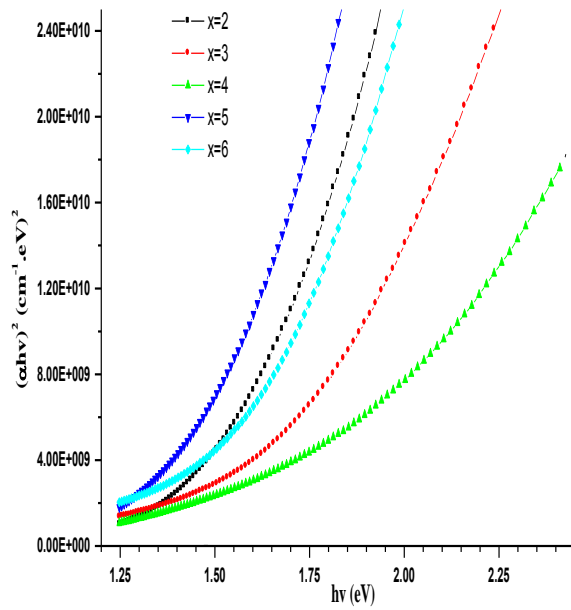


Fig (4.9)

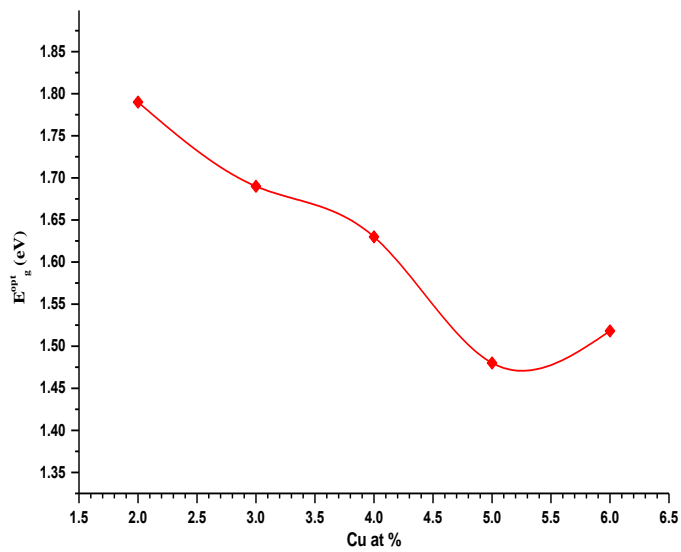


Fig. (4.10)

Fig.(4.8.a, b,c,d and e) The dependence of $(\alpha h\nu)^2$ on photon energy ($h\nu$) for all five samples respectively, from which the optical band gap is estimated (Taucs extrapolation).

Fig. (4.9) The dependence of $(\alpha h\nu)^2$ on photon energy ($h\nu$) for the five samples of Ge-Te-Cu thin films, the shift in the curve with changing Cu content is observed clearly in this figure.

Fig. (4.10) The variation of optical energy gap with Cu content for the five samples of Ge-Te-Cu thin films.

amorphous semiconductors. According to the model described by Kastner [73] and the electronic structure calculated by D.W. Bullet [74], the dominant contribution for states near the valance band edge in materials having chalcogenide atoms as major constituents comes from chalcogenide, especially from the chalcogenide lone-pair p-orbital. The lone-pair electrons in chalcogenide atoms adjacent to electropositive atoms which will have higher energies than those close to electronegative atoms. Therefore, the addition of electropositive elements to the alloy may raise the energy of some lone-pair states sufficiently to broaden further the band to the inside of the forbidden gap. The electronegativities of Ge, Te and Cu are 1.8, 2.1 and 1.9 (Pauling scale), respectively. According to these values we can notice that Ge is less electronegative than Cu, so the substitution of Cu for Te is expected to raise the energy of lone-pairs states and hence to broaden the valance band [75].

This composition, $x=5$ at.% can be considered as a critical composition at which the system becomes a chemically ordered alloy. It was found that at further addition of copper, E_g^{opt} values start increasing again. Further addition of Cu ($x > 5at. \%$) favors the formation of Cu-Cu bonds (2.012 eV) thus reducing the Cu-Te bond concentration. This in turn results an increasing bond energy and hence the cohesive energy which results in the increase of E_g^{opt} . The obtained results were found to be in good agreement with the results obtained in references [59,75].

The constant β is almost independent on the chemical composition and in a good agreement with the values of the chalcogenide semiconductor films studied before, and the average value has been found to be equal to $5.25 \times 10^5 eV^{-1} cm^{-1}$ most of β values being within range of this mean value [25].

Table (4.1) Optical band gap, β constant and Urbach energy E_t as a function of Cu content for $Ge_{15}Te_{85-x}Cu_x$ ($2 \leq x \leq 6$ at. %) thin films.

Sample number	Composition at. %			E_g^{opt} (eV)	E_t (eV)	β ($cm^{-1}eV^{-1}$)
	Ge ₁₅	Te _{85-x}	Cu _x			
1	15	83	2	1.79	0.720	5.188×10^5
2	15	82	3	1.69	0.743	5.776×10^5
3	15	81	4	1.61	1.632	5.019×10^5
4	15	80	5	1.48	1.797	5.261×10^5
5	15	79	6	1.62	0.782	5.009×10^5

4.3.2. Determination of high frequency refractive index (n) of

$Ge_{15}Te_{85-x}Cu_x$ thin films

The transmittance $T(\lambda)$ and absorption $A(\lambda)$ for the compositions $Ge_{15}Te_{85-x}Cu_x$ thin films have been used to compute the refractive index n using equation (2.24). The spectral dependence of n for $Ge_{15}Te_{85-x}Cu_x$ thin films is shown in figure (4.11).

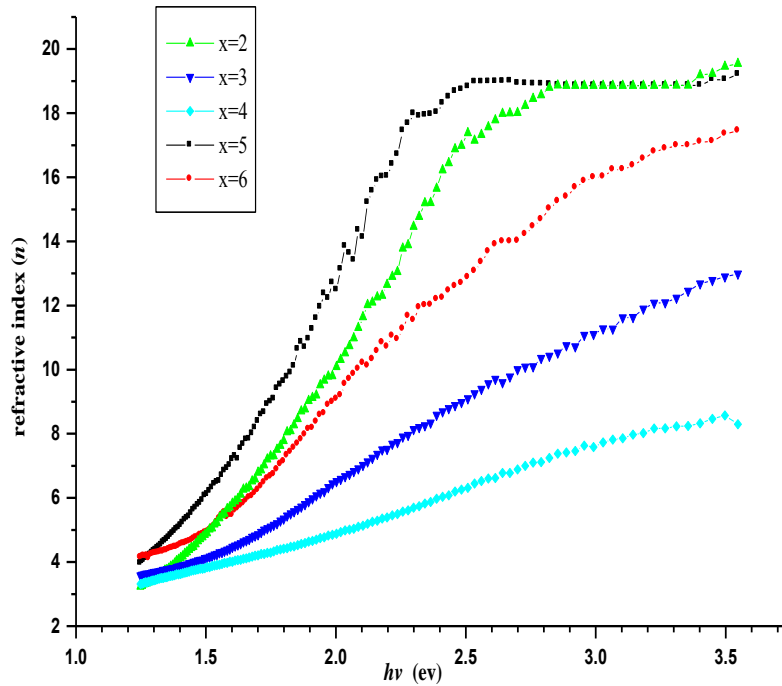


Fig.(4.11) Variation of refractive index(n) with photon energy $h\nu$ (eV) for $\text{Ge}_{15}\text{Te}_{85-x}\text{Cu}_x$ thin films of compositions.

It could be seen that the refractive index n increases with increasing photon energy, in contrast the refractive indices n decreases linearly with increasing wavelength for the thin films, indicating the typical shape of the dispersion curve near an electronic interband transition.

It is clear from figure (4.11) that n increases with increasing Cu content, the sample with copper content $x = 5$ has highest values of refractive index, which is makes Ge-Te-Cu chalcogenide films very attractive candidates as optical recording material [6].

4.3.3. Analysis of refractive index (high frequency dielectric constant and ratio of carrier concentration (N/m^*) for $\text{Ge}_{15}\text{Te}_{85-x}\text{Cu}_x$ films)

The real ε_r' and imaginary ε_r'' parts of the dielectric constant and the ratio of the carrier concentration N/m^* were obtained using following equations

$$\varepsilon_r' = n^2 - k^2 = \varepsilon_\infty - \left(\frac{e^2}{\pi c^2}\right) \left(\frac{N}{m^*}\right) \lambda^2 \quad (4.2.a)$$

$$\varepsilon_r'' = 2nk \quad (4.2.b)$$

where n , is the refractive index, ε_∞ is the high frequency dielectric constant, c is the velocity of the light, e the electron charge, and N/m^* is the ratio of free carrier concentration (N) to the free carrier effective mass (m^*). The real part dielectric constant is associated with the term that how much it will slow down the speed of light in the material and the imaginary part gives that how a dielectric absorbs energy from electric field due to dipole motion [76].

Figures (4.12) and (4.13), show the variation of the real and imaginary parts of dielectric constants respectively with photon wavelength (nm)

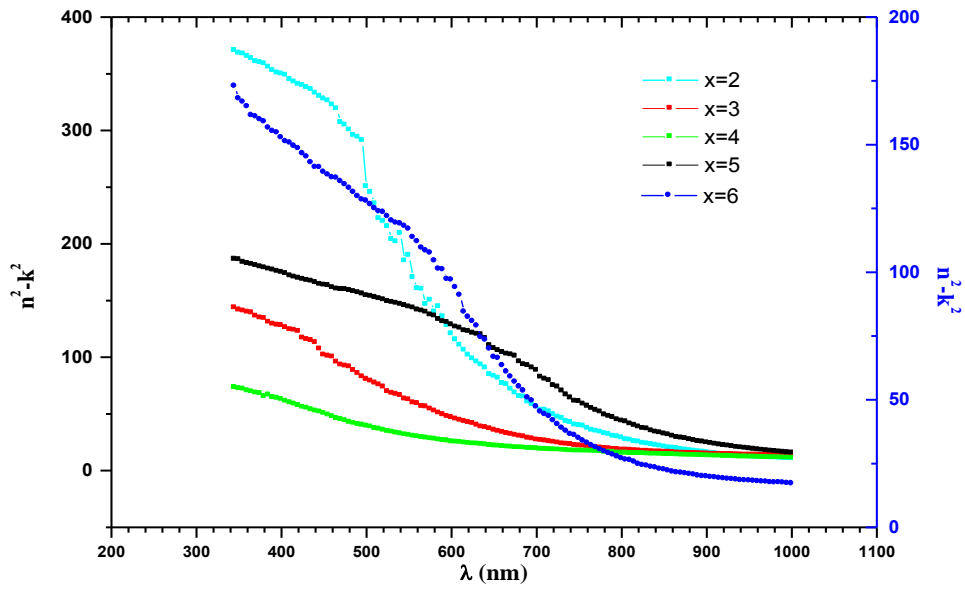


Fig.(4.12) Variation of real part of dielectric constant n^2-k^2 with wavelength λ (nm) of $\text{Ge}_{15}\text{Te}_{85-x}\text{Cu}_x$ thin films of compositions.

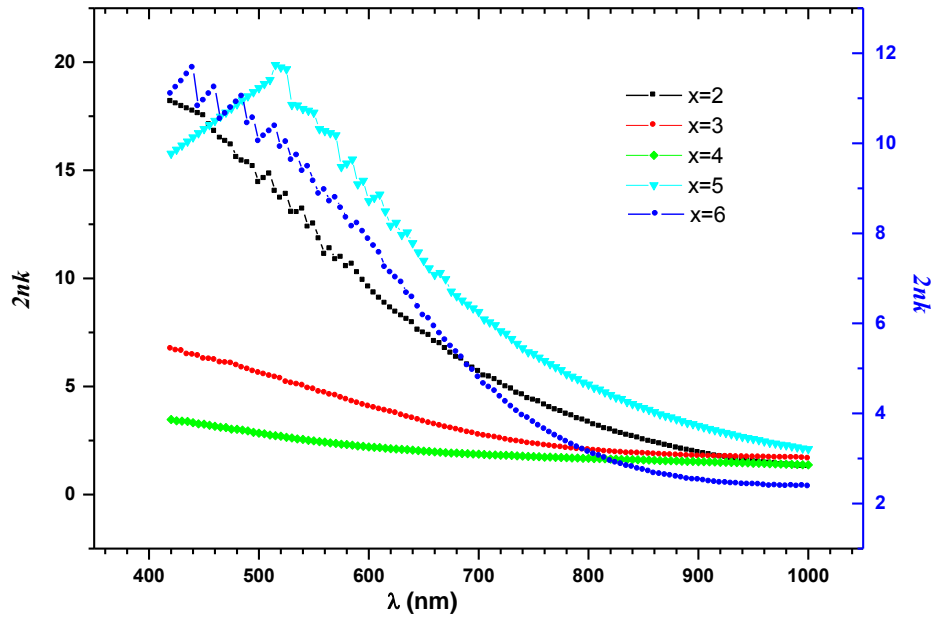


Fig.(4.13) Variation of imaginary part ($\epsilon_r=2nk$) of dielectric constant with wavelength λ (nm) for $\text{Ge}_{15}\text{Te}_{85-x}\text{Cu}_x$ thin films of compositions.

The obtained data for the refractive index can be analyzed to obtain the high frequency dielectric constant via two procedures. The first procedure describes the contribution of free carriers and the lattice-vibration modes of dispersion. The second procedure, on the other hand, is based upon the dispersion arising from the bound carriers in an empty lattice. To obtain a reliable value for the high frequency dielectric constant both procedures were employed. In the first procedure, high frequency dielectric constant ϵ_{∞} and ratio of the carrier concentration N/m^* were obtained. The square of the refractive index n^2 was plotted versus λ^2 as shown in figure (4.14) for all samples. It was observed that the dependence of n^2 on λ^2 is linear at longer wavelength [68].

The values of ϵ_{∞} and the ratio of the carrier concentration N/m^* were deduced from the extrapolating the linear part of this dependence to zero wavelength $\lambda^2 = 0$ and from the slope of the graph respectively for all studied samples as shown in figure (4.15).

The obtained values of ϵ_{∞} and N/m^* for the $\text{Ge}_{15}\text{Te}_{85-x}\text{Cu}_x$ ($2 \leq x \leq 6$ at.%) thin films are listed in the table (4.2). It could be noticed that the dielectric constant and the ratio N/m^* decrease with increasing Cu content. This result agrees with that obtained by M. Dongol et al [71].

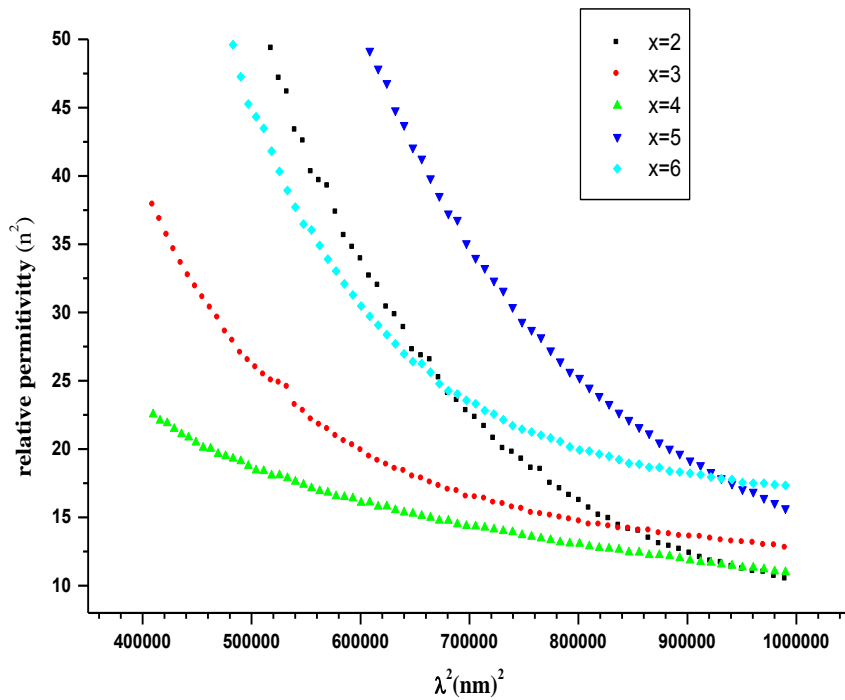


Fig.(4.14) Variation of relative permittivity with wavelength λ^2 (nm^2) for $\text{Ge}_{15}\text{Te}_{85-x}\text{Cu}_x$ thin films of compositions.

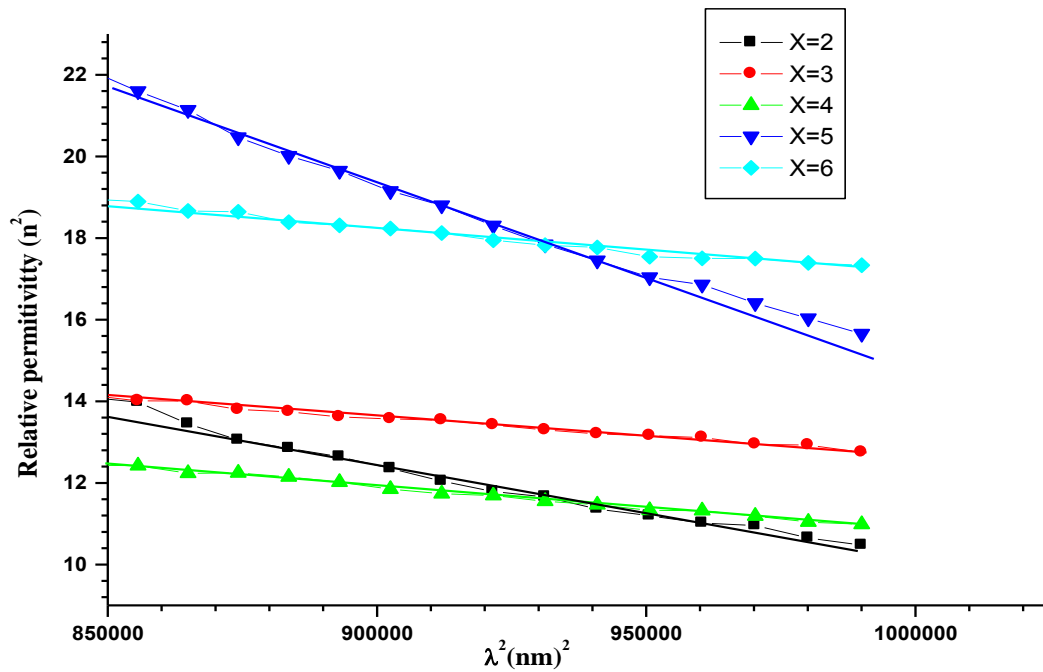


Fig.(4.15) Linear fitting of relative permittivity with the square of wavelength λ^2 (nm^2) for $\text{Ge}_{15}\text{Te}_{85-x}\text{Cu}_x$ thin films of compositions.

Table (4.2) The dielectric constant and the ratio N/m^* as a function of Cu content for $Ge_{15}Te_{85-x}Cu_x$ ($2 \leq x \leq 6$ at. %) thin films.

Sample Number	Composition at. %			Dielectric constant ϵ_{∞}	N/m^* (cm^{-3})
	Ge ₁₅	Te _{85-x}	Cu _x		
1	15	83	2	13.8	2.1569×10^{15}
2	15	82	3	14.2	1.02177×10^{14}
3	15	81	4	16.5	1.09499×10^{14}
4	15	80	5	19.8	4.3128×10^{14}
5	15	79	6	17	1.08201×10^{14}

In general, it can be concluded that N/m^* is related to the internal microstructure as can be emphasized by icon increases with increasing the copper content. This behavior has been observed in many chalcogenide glasses.

In the second procedure and at high frequencies, the properties of studied films could be treated as treated as a single oscillator at certain frequency (ν). The dispersion of refractive index (spectral dependence) has been analyzed in terms of Wemple-DiDomenico (WDD) model which is based on single effective oscillator approach see equation (2.25) [68]. The values of the parameters E_0 and E_d were obtained from the intercept and the slope and intercept resulting from the extrapolation of the curve of figure (4.17), which presents the plot of $(n^2 - 1)^{-1}$ versus $(h\nu)^2$ and

fitting the relation to a straight line for $\text{Ge}_{15}\text{Te}_{85-x}\text{Cu}_x$ films, as shown in figure (4.17).

The obtained values of E_0 and E_d are listed in table (4.3). It was observed that the single-oscillator energy and the dispersion energy varies with the Cu content. The oscillator energy, E_0 , is the average energy gap parameter and with a good approximation it varies in proportion to optical band gap ($E_0 \approx 2 E_g^{opt}$) [44].

The variation of E_0 and E_d with Cu concentration of the investigated compositions are shown in figure (4.18). The dispersion energy or single-oscillator strength, E_d , serves as a measure of the strength of interband transitions. It is observed that the variation in the transition strength, E_d , results primarily from changes in the nearest neighbor coordination number.

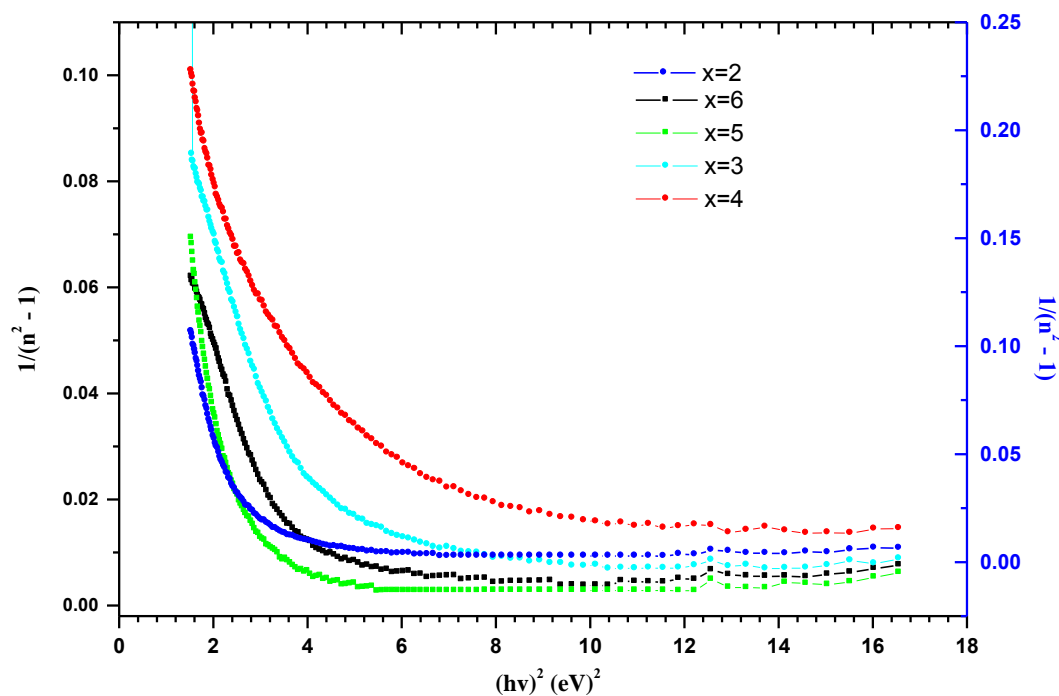


Fig.(4.16) Variation of refractive index factor $(n^2 - 1)^{-1}$ with $(hv)^2$ (eV)² for $\text{Ge}_{15}\text{Te}_{85-x}\text{Cu}_x$ thin films of compositions.

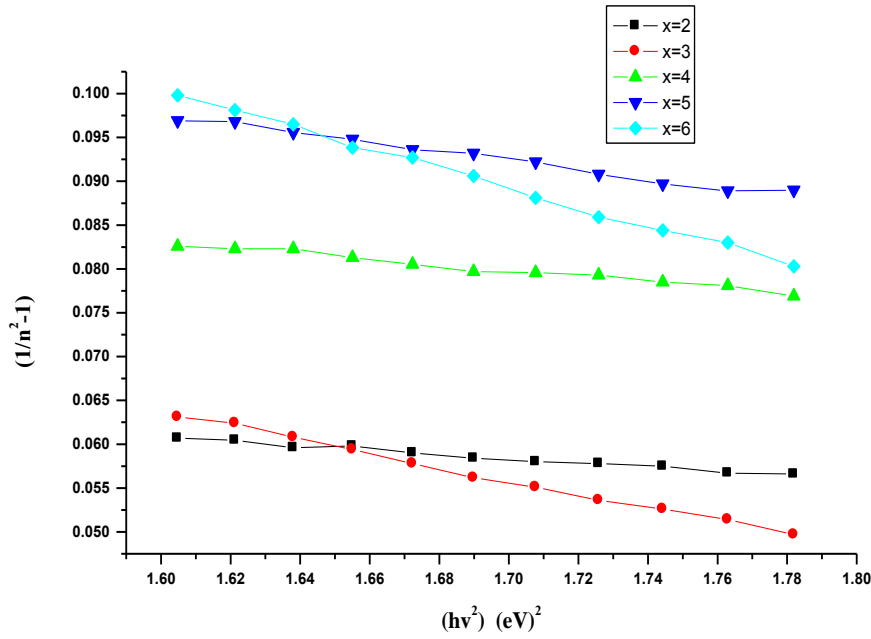


Fig.(4.17) Linear fitting for the variation of $(1/n^2-1)$ with $(hv)^2$ for $Ge_{15}Te_{85-x}Cu_x$ thin films.

Table(4.3) Wemple–DiDomenico dispersion parameters (E_0 and E_d), E_0/E_g^{opt} ratio as a function of Cu content for $Ge_{15}Te_{85-x}Cu_x$ ($2 \leq x \leq 6$ at. %) thin films.

Sample Number	Composition at (%)			E_g^{opt}	E_0 (eV)	E_d (eV)	E_0/E_g^{opt}
	Ge ₁₅	Te _{85-x}	Cu _x				
1	15	83	2	1.79	3.00	24.14	1.679
2	15	82	3	1.69	3.73	17.38	2.207
3	15	81	4	1.61	3.72	15.05	2.304
4	15	80	5	1.48	2.57	17.34	1.736
5	15	79	6	1.62	3.51	29.34	2.166

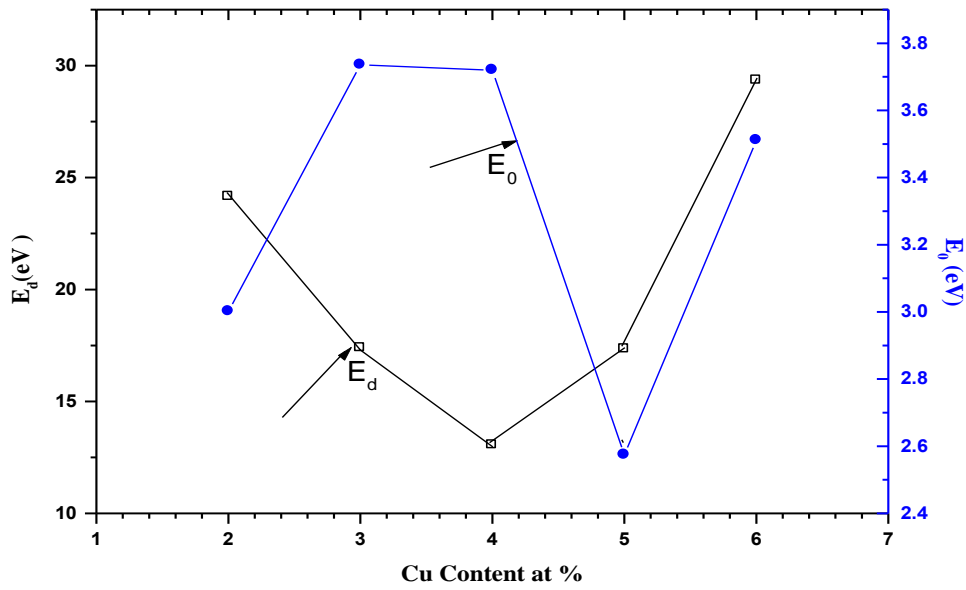


Fig.(4.18) Variation of Wemple- Di Domenico parameters E_o and E_d as a function of composition of Cu content for $Ge_{15}Te_{85-x}Cu_x$ thin films.

It was observed that the single-oscillator energy decreases while the dispersion energy increases with the increase of Cu content as shown in figure (4.18). The oscillator energy, E_o , is the average energy gap parameter and was found to be in a quite close approximation to the optical band gap ($E_o \approx 2E_g^{opt}$) [35].

4.4. Interpretation of the physical proprieties of $Ge_{15}Te_{85-x}Cu_x$ thin films and their dependence on energy

4.4.1. Average coordination number and the optical energy gap

In the recent years, topological models based on the constraints theory have been adopted for understanding the structure of covalent glasses as a function of the average coordination number [77,78]. The

chalcogenide glass systems generally show a critical average coordination of atoms called rigidity percolation threshold and the material experiences changes in its structural rigidity. The rigidity percolation and the ordering of the system are expressed by the anomalous properties of the system at the critical composition. By comparing the degrees of freedom of atoms with the number of the linear independent constraints, a notion of under constrained (rigid) amorphous solid was introduced. At $\langle r \rangle = 2.4$, the two quantities are equal and the structure of the glasses percolates. At this critical composition corresponding to $\langle r \rangle = 2.4$ the rigidity percolation occurs as suggested by Phillips and Thorpe [77,78]. The average coordination number $\langle r \rangle$, is a measure of connectedness and is linked with the number of bonds per atom in the network.

of the Ge-Te-Cu system is calculated using Fouad's approach [79]:

$$\langle r \rangle = [15 \text{CN}(\text{Ge}) + (85 - X)\text{CN}(\text{Te}) + X\text{CN}(\text{Cu})]/100 \quad (4.2)$$

where $\text{CN}(\text{Ge})$ is the coordination number of germanium, $\text{CN}(\text{Te})$ is the coordination number of tellurium, $\text{CN}(\text{Cu})$ is the coordination number of copper, X and $(85 - X)$ [are their respective atomic concentrations in the glassy alloy.

The values of $\langle r \rangle$ were calculated for all samples, see table (4.3). The variation of optical energy gap with average coordination number is plotted in figure (4.19), which shows that at $\langle r \rangle = 2.4$ a change of slope or a kink is observed generally in as expected in chalcogenides.

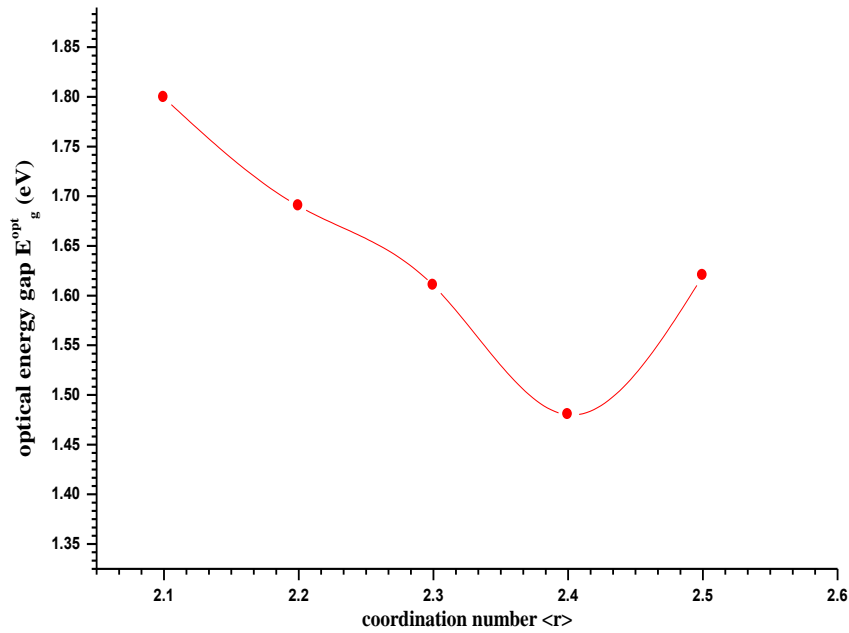


Fig. (4.19) Variation of optical energy gap E_g^{opt} with average coordination number $\langle r \rangle$ for $\text{Ge}_{15}\text{Te}_{85-x}\text{Cu}_x$ thin films of compositions.

4.4.2. Average heats of atomization and the optical energy gap

It is interesting to relate the optical gap with the average heat of atomization. The optical properties of our composition is dependence on chemical composition are also of interest, especially in considering the effects of average coordination number, $\langle r \rangle$, of covalent bonds per atom. We noticed that, the average heat of atomization H_s [in $\text{Kcal}/(\text{g atom})^{-1}$] is defined as a direct measure of cohesive energy. The calculated values of H_s for the prepared compositions were calculated using equations (2.26) and (2.28), and were listed in table (4.3).

The increases in H_s with increasing the Cu content can be attributed to the fact that the average binding energy of the composition is increased, so it is reasonable that the optical gap decreases.

We noticed that from Table (4.3), the average coordination number for $\text{Ge}_{15}\text{Te}_{85-x}\text{Cu}_x$ ($2 \leq x \leq 6$, at. %) thin films increases with increasing the Cu content.

The optical gap reflects the separation of the top of the filled lone-pair p-states of the valance band from the bottom of the antibonding states in the conduction band. It is, therefore, interesting to relate the optical band gap with the chemical bond energy. For this purpose we used two parameters that specify the bonding, the average coordination number and the average heat of atomization. In order to emphasize the relationship between E_g^{opt} and the average band strength more clearly, E_g^{opt} is compared with $H_s / \langle r \rangle$ which is the average single-bond energy in the alloy. Figure (4.20) shows the variation of $H_s / \langle r \rangle$ and E_g^{opt} with the average coordination number.

The results indicate that the heat of atomization H_s and the optical energy gap E_g^{opt} decreases with increasing the coordination number. Furthermore, these results indicate that there are important correlation between E_g^{opt} , H_s and $\langle r \rangle$, this means that the heat of atomization and the average coordination number could be considered as the main factors to characterize the optical energy gap.

Figure (4.20) shows that at the same point $\langle r \rangle = 2.4$ (corresponding to the Cu content, $x=5\%$) a change of slope or a kink was observed, this agrees with Phillips and Thorpe [77,78] suggestion that the system undergoes a transition from one-dimensional polymeric to a layer structure and become rigid. Hence the composition with 5% Cu can be considered as a critical one. At this rigidity percolation point, a chemical ordering also occurs in the network.

Table (4.4) The values of atomization energy H_s , coordination number $\langle r \rangle$ and the ratio $H_s/\langle r \rangle$ as a function of Cu content for $Ge_{15}Te_{85-x}Cu_x$ ($2 \leq x \leq 6$ at. %) thin films.

Sample Number	Composition at .%			E_g^{opt} (eV)	H_s (Kcal/g.atom ⁻¹)	$\langle r \rangle$	$H_s/\langle r \rangle$
	Ge ₁₅	Te _{85-x}	Cu _x				
1	15	83	2	1.79	52.88	2.1	25.18
2	15	82	3	1.69	53.24	2.2	24.20
3	15	81	4	1.61	53.59	2.3	23.30
4	15	80	5	1.48	53.95	2.4	22.48
5	15	79	6	1.62	54.05	2.5	21.62

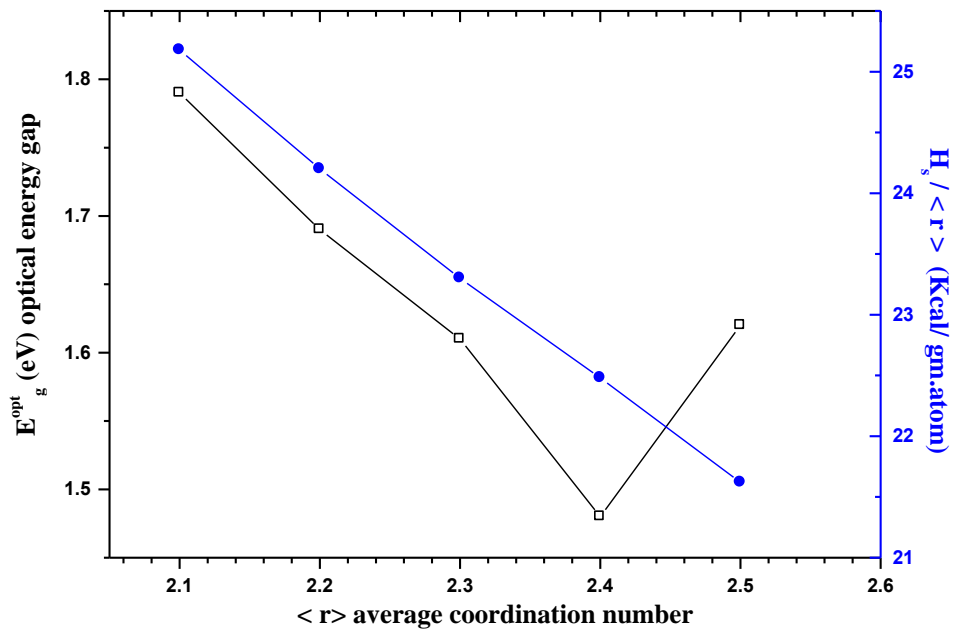


Fig. (4.20) The optical gap E_g^{opt} and the average heat of atomization per single bound $H_s/\langle r \rangle$ as a function of average coordination number for $Ge_{15}Te(85-x)Cu_x$ thin films.

Following conclusions were drawn from the past analysis

- 1- X-ray diffraction technique was used to check the amorphisation and homogenization of the ternary Ge-Te-Cu system. The obtained films were found to be in an amorphous state.
- 2- From the figures obtained in the present study it may be concluded that both n and k vary with Cu content and show higher values at Cu concentration $x=5$ at.%.
 $n = 1.48$ at concentration Cu=5 at.%.
- 3- The optical absorption is due to allowed direct transitions and the band tail width obeys the Urbach empirical relation.
- 4- The optical band gap is appropriately fitted to the allowed direct transition proposed by Tauc. The results indicate that E_g decreases with increasing in Cu content and reaches a minimum value of $E_g = 1.48$ at concentration Cu=5 at.%.
- 5- Analysis of the refractive index yields the high frequency dielectric constant and n/k ratio, which were found to increase with increasing in Cu content.
- 6- We have analyzed in detail the optical-dispersion data, using the insightful WDD single-oscillator model, it was observed that the single –oscillator energy decreases while the dispersion energy increases with the increase of Cu content.

- 7- The results indicate that χ increases with incensement in Cu content, and $\langle r \rangle$ were correlated to .
- 8- It was found that at $\langle r \rangle = 2.40$ corresponds to the sample with composition of Cu x=5 at.%, this composition $\text{Ge}_{15}\text{Te}_{80}\text{Cu}_5$ can be considered as a **critical composition**, where we can observe changes in all optical constants and at which the system becomes a chemically ordered alloy. Chalcogenide systems of the average coordinate number $\langle r \rangle = 2.40$ undergo the least number of configurational rearrangements in transforming to a glass and is the most connected network, hence, such compositions are the **best glass-formers**.

References

- [1] Raouf A. H. El-Mallawany, Hand Book Physical Properties and Data, CRC Press, Florida, USA (2000).
- [2] S.R. Elliott, Physics of Amorphous Materials, 2, Longman, London, 1990.
- [3] N. Ramesh Rao, P.S.R. Krishna, S. Basu, B.A. Dasannacharya, K.S. Sangunni and E.S.R. Gopal, J. Non-Cryst. Solids 240 (1998) 221.
- [4] E. Marquez, T. Wagner, J.M. Gonza'lez-Leal, A.M. Bernal-Olive, R. Prieto-Aleon, R.J. Imenez-Garay and P.J.S. Ewen, J. Non-Cryst. Solids. 274 (2000) 62.
- [5] V.A. Twaddell, W.C. Lacourse, J.D. Mackenzie, J. Non-Cryst. Solids 8 (1972) 831.
- [6] K.S. Liang, A. Bienenstock and C.W. Bates, Phys. Rev. 10 (1974) 1524.
- [7] Z.M. Sateh, G.A. Williams and P.C. Taylor, Phys. Rev. 40 (1989) 10557.
- [8] Arun K. Varshneya, J. Non-Cryst. Solids 273 (2000) 1.
- [9] Jamers D. Patterson and Bernard C. Bailey, Solid State Physics, Springer-Verlag Berlin Heidelberg, Berlin, (2007).
- [10] J. Tauc, R. Grigorovici and A. Vancu, Phys. Stat. Sol. 15 (1966) 627.
- [11] F. Urbach. Phys. Rev. 92 (1953) 1324.
- [12] J.C. Manifacier, J. Gasiot, J.P. Fillard, J. Phys., E.J. Sci. Instrum. 9 (1976) 1002.
- [13] R.Swanpoel, J. Phys., E.J. Sci. Instrum. 16 (1983) 1214.
- [14] S.H. Wemple, M. DiDomenico, Phys. Rev. B3 (1971) 1338.
- [15] S.H. Wemple, Phys. Rev. B7 (1973) 3767.
- [16] R. Swanpoel, J. Phys., E J. Sci. Instrum. 17 (1984) 896.
- [17] E.R. Shaaban, N. El-Kabnay, A.M. Abou-sehly, N. Afify, Physica 381 (2006) 24.

- [18] J.M. González-Leal, R. Prieto-Alcón, M. Stuchlik, M. Vlcek, S.R. Elliott, E. Márquez, *Opt. Mater.* 27 (2004) 147.
- [19] Mark Fox, *Optical Properties of Solids*, Oxford University Press, New York, (2001).
- [20] Driscoll, W.G. and Vaughan, W. (1978). *Handbook of optics*. McGrawHill, New York
- [21] Charles Kittel, *Introduction to Solid State Physics* (Eighth edition), John Wiley & Sons, Canada (2005).
- [22] G. Saffarini, J.M. Saiter, H. Schmitt, *Optical Materials* 29 (2007) 1143.
- [23] R.A. Street, *Hydrogenated Amorphous Silicon*, Cambridge University Press, Cambridge (1991).
- [24] D.A. Papaconstantopoulos, E.N. Economou, *Phys. Rev.B* 24(1981) 7233.
- [25] M.H. Cohen, H. Fritzsche, and S.R. Ovshinsky, *Phys. Rev.* 1065 (1969) 22.
- [26] N.F. Mott and E.A. Davis, *Electronic Processes in Non-crystalline Materials*, Clarendon Press, Oxford (1979).
- [27] S.K. O’Leary, S.R. Johnson, and P.K. Lim, *J. Appl. Phys.* 82 (1997) 3334.
- [28] S.M. Malik and S.K. O’Leary, *J. Non-Cryst. Solids*, 64 (2004) 336.
- [29] S. Sherman, S. Wagner, and R.A. Gottscho, *Appl. Phys. Lett.* 69 (1996) 3242.
- [30] Jai Singh, *Optical Properties of Condensed Matter and Applications*, John Wiley & Sons, England (2006).
- [31] J. Tauc, *The Optical Properties of Solids*, edited by F. Abeles North-Holland, Amsterdam (1979).
- [32] J. Tauc, In *Amorphous and Liquid Semiconductors*, ED. J. Tauc, Plenum Press, New York (1974).
- [33] A.A. Al-Ghamdi, *Vacuum* 80 (2006) 400.
- [34] H. El-Zahed, M. Dongol, M. Radwan, *Eur. Phys. J.* 17 (2002) 179.
- [35] E.A. Mahmoud, M.M. El-Samanoudy, A.S. Abd Rabo, *Journal of Physics and Chemistry of Solids* 63 (2002) 2003.
- [36] K. A.Aly, H.H. Amer, A. Dahshan, *Material Chemistry and Physics* 113 (2009) 690.
- [37] A.S. Abd-Rabo, K.A. Sharaf, *Journal of Pure and Applied Physics* 3 (2007) 49.
- [38] J.D. Dow, D. Redfield, *Phys. Rev. B* 5 (1972) 594.
- [39] M. Zanini, J. Tauc, *J. Non-Cryst. Solids* 23 (1977) 349.
- [40] E.A. Davis, N.F. Mott, *Philos. Mag.* 22 (1970) 903.
- [41] Y. Tawada, K. Tsuge, M. Kondo, H. Okamoto, Y. Hamakawa, *J. Appl. Phys.* 53 (1982) 5273.

- [42] H.A. MacLeod, *Thin Film Optical Filters*, Adam Hilger Macmillan, London, New York, (1987).
- [43] K.A. Aly, A.M. Abousehly, M.A. Osman, A.A. Othman, *Journal Physica B* 403 (2008) 1848.
- [44] El-Sayed, M. Farg, *Optica & Laser Technology* 38 (2006) 14.
- [45] L. Pauling, *J. Phys, Chem.* 58 (1954) 662.
- [46] S.C Agarwal, M.A Paesler, D.A. Baker, P.C. Taylor, G. Lucovsky and A. Edwards, *Pramana Journal of Physics.* 70 (2008) 245.
- [47] J.C. Phillips, *J. of Non-Cryst. Solids* 153 (1979) 34.
- [48] A.H. Ammar, A.M. Farid and S.S. Fouad, *Physica B* 307(2001)64.
- [49] K. Ramesh, S. Asokan, K.S. Sangunni, E.S.R. Gopal, *Journal of Physics and Chemistry of Solids* 61 (2000) 95.
- [50] A.F. Loffe, A.R. Regwl, *Prog. Semicond.* 4 (1960) 239.
- [51] V.M. Goldschmidt, *Trans. Faraday Soc.*, 25 (1926) 253.
- [52] I. S. Dutsyak, *Tech. Phys, (USA)*, 42 (1977) 1053.
- [53] A.H. Ammar, *Applied Surface Science*, 201(2002) 9.
- [54] M. Kastner, *Phys.Rev.Lett.*28 (1972) 355.
- [55] Afaf A. Abd El-Rahman, A.M. Eid, M. Sanad, and R.M. El-Ocker, *J. Physics. Chem. Solids* 59 (1996) 825.
- [56] H.E. Atiya, A.E. Bekheet , *Physica B* 403 (2008) 3130.
- [57] M.M. Abdel-Aziz, E.G. El-Metwally, M. Fadel, H.H. Labib, M.A. Afifi, *Thin Solid Films.* 386 (2001) 99.
- [58] N.F. Mott, E.A. Davis, *Electronic Processes in Non-Crystalline Materials*, Clsrendon, Oxford, (1971).
- [59] Pankaj Sharma , S.C. Katyal, *Thin Solid Films* 515 (2007) 7966.
- [60] E.R. Shaaban, *Journal of Physics and Chemistry of Solids* 68 (2007) 400.
- [61] M. Dongol, M. Abou Zied, G.A. Gamal, A. EI-Denglawey, *Physica B.* 353 (2004) 169.
- [62] A.B. Abd-El-Moiz, M.M. Hafiz, A.H. Oraby and M. Dongol, *Physica B* 217 (1996) 265.
- [63] D.D. Strbac, S.R. Lukic, D.M. Petrovic, J.M. Gonzalez-Leal and A. Srinivasan *Journal of Non-Crystalline Materials* 353 (2007) 1466.
- [64] J.M. Gonzalez-Leal, R. Prieto-Alcon, J.A. Angel, and M. Marquez, *J. Non-Cryst. Solids* 315 (2003) 134.
- [65] N.El-Kabany, *Physica B.* 403 (2008) 2949.
- [66] N. El-Kabany, E.R. Shaaban, N. Afify and A.M. Abou-Sehly, *Physica B.* 403 (2008) 31.
- [67] M. Krbal, T. Wagner, Mil. Vlcek, Mir. Vlcek, M. Frumar, , *J. Non-Cryst. Solids,* 352 (2006) 2662.
- [68] W.B. Jackson, S.M. Kelso, C.C. Tsai, J.W. Allen, and S.-H. Oh, *Phys. Rev. B* 31 (1985) 5187.

- [69] A.E. Bekheet , N.A. Hegab, M.A. Afifi, H.E. Atyia, E.R. Sharaf, Applied Surface Science 255 (2009) 4590.
- [70] S. A. Fayek, L.A. Wahab, S. M. El-Sayed and A. H. Ashour, Vacuum, 49 (1998) 59.
- [71] L.A. Wahab, H.H. Amer, Materials Chemistry and Physics 100 (2006) 430.
- [72] M. Dongol, M. AbouZied, G.A. Gamal, A. El-Denglawey, Appl. Surf. Sci. 161 (2000) 365.
- [73] C. Harikuttan Unnithan, P. Predeep, S. Jayakumar, Journal of Physics and Chemistry of Solids 64 (2003) 707.
- [74] S.A. Fayek, S.M. El-Sayed, Materials Chemistry and Physics 71 (2001) 226.
- [75] G.A.M. Amin , A.F. Maged, Materials Chemistry and Physics 97 (2006) 420.
- [76] Pankaj Sharma and S.C. Katyal, Materials Chemistry and Physics, 112 (2008) 892.
- [77] J.C. Phillips, J. Non-Cryst.Solids 34 (1979) 153.
- [78] M.F. Thorpe, J. Non-Cryst.Solids 57 (1983) 355.
- [79] S.S. Fouad, J. Phys. D Appl. Phys. 28 (1995) 2318.

ملخص الرسالة

تهدف هذه الدراسة إلى الحصول على نتائج حول تأثير تغيير التركيب لأغشية رقيقة مختلفة التكوين من الجيرمانيوم-تيلوريوم-نحاس ($Ge_{15}Te_{85-x}Cu_x$ ($2 \leq x \leq 6$)) على الخواص الضوئية والالكترونية لها ولعل الهدف الأساسي من هذه الدراسة هو تطوير فهم طبيعة أشباه الموصلات الأم ورفية وأيضا للحصول على أكبر قدر من الثوابت الضوئية والالكترونية عن طريق الدراسة العملية والنظرية من طيف الامتصاص والنفذية لهذه العينات، ومن ثم تعيين العينة الأكثر كفاءة لاستخدامها في الدوائر الالكترونية .

وقد تم تحضير خمس عينات من $Ge_{15}Te_{85-x}Cu_x$ ($2 \leq x \leq 6$) (بتركيزات مختلفة للنحاس والتيلوريوم) بطريقة التبخير الحراري. وللتحقق من الطبيعة الأمورفية للعينات تم اجراء قياسات حيود الأشعة السينية $X-ray diffraction$ التي اكدت أن العينات جميعا كانت في الحالة الأمورفية. ولدراسة خواص العينات الضوئية تم قياس طيف الامتصاص والنفذية لهذه العينات في المدى 280-1000 nm ، ومنه حسبت بعض الثوابت الضوئية كقيمة فجوة الطاقة الضوئية E_g ، عرض الحالات المحلية ، معامل الانكسار ، معامل التخميد ، والجزء التخيلي والحقيقي لثابت العزل. ولقد وجدنا في الدراسات الطيفية ان الانتقال الالكتروني المباشر المسموح هو الانتقال المسؤول عن الامتصاص الضوئي وفسر هذا باستخدام علاقة $Tauc's relation$. ولقد وجد ان فجوة الطاقة الضوئية تصل إلى قيمة دنيا عند تركيز عنصر النحاس $x=5$ ، وسمي هذا التركيز بالتركيز الحرج $critical\ composition$.

تم دراسة تشتت معامل الانكسار في ضوء نموذج ويمبل دي دومينيك $Single-Oscillator$ $Wemple\ and\ DiDomenico\ Model$ حيث تم حساب قيمة كل من طاقة التشتت وطاقة المتذبذب وعلاقتهم بفجوة الطاقة الضوئية.

ولدراسة علاقة طاقة الفجوة الضوئية بالتركيب الكيميائي للعينات المحضرة تم حساب متوسط الطاقة الذرية ومتوسط رقم الاحداثي وربط هذه القيم بقيم طاقة الفجوة الضوئية. وقد أظهرت النتائج أن متوسط الطاقة الذرية يزيد يقل بزيادة عنصر النحاس، وانه عند تركيز نحاس $x=5$ متوسط رقم احداثي يساوي 2.40 . هذا التركيز يعتبر التركيز الحرج الذي نجد تغيرات في جميع الثوابت الضوئية.

تم تفسير تغير طاقة الفجوة الضوئية بتغير التركيز باستخدام نظرية قيود الربط $Bond\ Constraint$ $Theory$ ونظرية الصلابة $Rigidity\ Theory$.



المملكة العربية السعودية
وزارة التعليم العالي
جامعة أم القرى
كلية العلوم التطبيقية
قسم الفيزياء

دراسة الخواص الضوئية
لأغشية رقيقة مختلفة التكوين
من الجرمانيوم-التيليريوم-النحاس

إعداد

غادة عبدالرحمن الزايدي

إشراف

د. ناهد أبو الحسن القباني

أ.د. أحمد حمزة عرابي

رسالة مقدمة إلى قسم الفيزياء بكلية العلوم التطبيقية بجامعة أم القرى
كمطلب تكميلي لبرنامج درجة الماجستير في الفيزياء